CONCURRENT APPROACH FOR RAPID PROCESS DEVELOPMENT AND ISOTHERM CHARACTERIZATION

A Dissertation
Presented to
The Academic Faculty

by

Siwei Guo

In Partial Fulfillment
of the Requirements for the Degree
Doctor of Philosophy in the
School of Chemical & Biomolecular Engineering

Georgia Institute of Technology
May 2018

CONCURRENT APPROACH FOR RAPID PROCESS DEVELOPMENT AND ISOTHERM CHARACTERIZATION

Approved by:

Dr. Sankar Nair, Advisor
School of Chemical & Biomolecular Engineering
Georgia Institute of Technology

Dr. Ryan P. Lively
School of Chemical & Biomolecular Engineering
Georgia Institute of Technology

Dr. Yoshiaki Kawajiri, Co-advisor
School of Chemical & Biomolecular Engineering
Georgia Institute of Technology

Dr. Sotira Yiacoumi
School of Civil and Environmental Engineering
Georgia Institute of Technology

Dr. David S. Sholl, Co-advisor
School of Chemical & Biomolecular Engineering
Georgia Institute of Technology

Date Approved: March 30, 2018

A wise man once said, “Research is a journey going from one failure to another with undiminished enthusiasm.” I dedicate this thesis to my parents who have been a great source of support and comfort during this journey.

ACKNOWLEDGEMENTS

There are many people to thank along the way in completing this thesis project. First, I would like to thank my Ph.D. advisors who lead me to the magical land of scientific research. I would like to thank Dr. Yoshiaki Kawajiri, from whom I learned to pay attention to details, analyze engineering situations with logic, and set a reasonable timeline for my projects. I would like to thank Dr. Sankar Nair, who has been a constant source of direction. Time and time again, Dr. Nair was able to draw a clear path and provide an insightful vision for the project. I would like to thank Dr. David Sholl, who is very knowledgeable of a variety of different areas. His wisdom always inspires me to aim higher.

I would like to thank Dr. Jason Bentley, who was a post-doc researcher at Georgia Tech when I started my work. I am beyond words of gratitude for Jason's help to kick start my research. Jason was willing to spend hours tutoring me about modeling and experiments with tremendous patience.

I am also grateful to my colleagues, friends, and family. I want to thank Asch, who always calm me down, I want to thank Oliver, who always cheers me up, and I want to thank Xander, who teaches me to focus on my goals. I also want to thank Angela who helped me with almost everything in the past few years.

TABLE OF CONTENTS

LIST OF TABLES

LIST OF FIGURES

LIST OF SYMBOLS AND ABBREVIATIONS

Variables

A	a set that stores liquid compositions selected previously
b	adsorption constant
C	liquid concentration
D_L	axial dispersion coefficient
F^n	flow rate of zone n
f	scalar-valued function
$H_{i,k}$	Henry's constant of component i at iteration k
k^{ma}	mass transfer coefficient
L	total length of all SMB columns
M	multiplier for Tikhonov regulation
N_{COMP}	number of components
N_{EXP}	number of experiments
N_{ITER}	number of iterations
Q^{sat}	Saturation capacity
q^{eq}	equilibrium adsorbate concentration
q	adsorbate concentration
t	time
t_s	switching time
V_c	column volume
z	axial position

Greek letters

$\zeta_{p,k}$	binary variable
φ_k	variable for objective function
θ	variables for model parameters
ρ_{ads}	density of adsorbent
δ	tolerance

Subscripts

COMP	components
case	index for cases during model optimization
D	desorbent
dead	indicate dead volume properties
Ex	extract
EXP	experiments
Fd	feed
i	index for components
j	dummy index used in extended Langmuir isotherm
k	index for iterations (isotherm determination)
m	index for iterations (plant-specific parameter determination)
n	index for columns
Pur	purity
p	index for experimental measurements
Ra	raffinate
Rec	recovery

Superscripts

eq	equilibrium
MAX	largest number of a series or set
in	inlet
out	outlet
sat	saturation
*	optimal

SUMMARY

The design of simulated moving bed (SMB) separation processes is a challenging and time-consuming task, especially when competitive multicomponent adsorption is involved. This thesis project focuses on developing an alternative process design approach – the concurrent approach. This approach is proposed to predict the optimal SMB concentration profiles and operating conditions in an adsorption process and to simultaneously obtain isotherm parameters for multicomponent adsorption by selecting representative liquid compositions for experimental measurements. I demonstrate that the convergence of the concurrent method can be achieved in a few iterations with only a small number of multicomponent adsorption measurements. Then, I demonstrate a second iterative methodology to refine the SMB model by estimating the non-thermodynamic (i.e., mass transfer) and other (dead volume) system parameters, using only a very small number of runs on an SMB "mini-plant" designed and constructed in-house at Georgia Tech.

CHAPTER 1. INTRODUCTION

Chromatography is widely used in industry for the production of various high purity chemicals. In petroleum refining industry, chromatography processes are used to produce high purity *p*-xylene [1]. In the agro-food industry, fructose-glucose separation also adopts chromatography processes for adsorptive separation [2]. In the pharmaceutical industry, chromatography processes have enabled many highly selective separations [3, 4].

There are several advantages of chromatography processes. Chromatographic separation can be achieved based on a relatively small difference of physical or chemical properties that are not exploited in traditional separation processes. For example, component mixture with similar boiling points cannot be separated easily by traditional separation technologies such as distillation, but they can be separated efficiently by adsorptive separation where the separation does not depend on their boiling point. Chromatography processes can be used at low temperature to separate delicate chemicals such as perfumes, antibiotics, etc. [5-7]. Chromatography processes can also be used to recover high purity products for application where traditional separation technologies struggle with recovering high purity products[8-10]. In petroleum refining industry, *p*-xylene up to 99.9% purity can be produced using chromatography processes [11].

1.1 The Principle of Chromatography Processes

Chromatography processes consist of the mobile phase and the stationary phase. In general, the stationary phase can be a thin film coated on the inner surface of the column or solid particles tightly packed inside of the column. The material that is used as the stationary phase is referred to as the adsorbent. The mobile phase can be either liquid or gas which can carry a mixture of

components that travels through the column. In many applications of chromatography, the mixture of components is injected into the column directly without dilution.

The components in the mobile phase interact with the solid phase giving rise to the difference in retention times. Common mechanisms of separation include (1) size exclusion, (2) partitioning, (3) ion-exchange and (4) adsorption. The first mechanism, (1) size exclusion, usually occurs for microporous adsorbent where the kinetic diameter of mobile phase components is similar to the size of the micropores; the larger molecules that cannot enter the pores travels faster than smaller molecules that do enter the pores [12]. The second mechanism, (2) partitioning, is usually a liquid-liquid phase phenomenon; however, it represents another retention mechanism in chromatography. For example, in hydrophilic interaction chromatography (HILIC), a small amount of water is used in the mobile phase and is immobilized around the hydrophilic solid phase. The component mixture is separated due to the partitioning between the bulk eluent and a water-rich layer [13]. In the third mechanism, (3) ion-exchange chromatography, the mixture in the mobile phase and the stationary phase are both charged, and the components that carry the opposite charge of the stationary phase are retained more strongly in the stationary phase [14]. Finally, (4) surface adsorption phenomena is a mechanism utilized in many applications. In this mechanism, components in the mobile phase can form physical or chemical bonding to the surface of the solid phase. The stronger the bonding is, the more strongly retained the components are [15].

1.1.1 Preparative Chromatography

Chromatography processes can be categorized into analytical chromatography processes and preparative chromatography processes depending on their purposes.

For analytical chromatography processes, the amount of the feed mixture to be injected to the column should be as small as possible, since the objective is to analyze the sample but not to increase the productivity (throughput). Because the concentration is low, the adsorption behavior closely matches Henry's law (linear isotherm).

For preparative chromatography processes, on the other hand, the amount of the feed mixture to be injected into the column should be as large as possible to increase productivity. When the concentrations become high in the column, adsorption usually behaves *nonlinearly*, where the retention times of components are no longer constant but a variable depending on the concentration. This phenomenon is characterized as "overloading," and is traditionally avoided in analytical chromatography[15].

Overloading can lead to improved process productivity/throughput in many industrial processes if appropriately designed. For example, the component adsorbed more strongly can desorb the less strongly adsorbed component leading to the sharpening of the elution front [15]; and this is called the "self-displacement condition," which can lead to an increase in the productivity. The simulated moving bed processes (SMB) studies in this project are usually designed to operate in the "overloaded" range for maximum productivity. The undiluted feed is often used, and the adsorption equilibrium is measured in the nonlinear range.

1.2 **Simulated Moving Bed (SMB) Processes**

Continuous counter-current chromatography processes are usually preferred compared to batch processes because of better separation performance (higher productivity, less solvent consumption, etc.) [16]. An example of continuous counter-current chromatography is the

simulated moving bed (SMB) processes developed in the early 1970s by Universal Oil Products [17].

1.2.1 True Moving Bed (TMB) Processes

To understand the principles of SMB, this thesis first discusses its ideal counterpart: true moving bed (TMB) processes. In the TMB processes, there is a circulation of the liquid as well as a circulation of the solid. Figure 1 shows a schematic of the TMB processes. In TMB processes, liquid circulates counter-clockwise, while the solid (adsorbent, or stationary phase) circulates clockwise. The solvent that is used to desorb components in the stationary phase is called the desorbent. The solid used in the TMB is called adsorbent. The feed contains a mixture of components. The component(s) that adsorb strongly on the adsorbent is referred to as the heavy component which is collected in the extract stream. The component(s) that is retained less strongly on the adsorbent is referred to as the light component(s), which is collected in the raffinate stream. Desorbent, extract, raffinate, and feed separate the column into four zones. In Zone I, fresh desorbent comes in to "wash" the adsorbent, and thus this zone is also called the "Desorption Zone". In Zone II, the lighter components are stripped away leaving high purity heavy components, which is also called the "Purification Zone". In Zone III, the heavy components are depleted, and the lighter components are enriched, and Zone III is thus called the "Adsorption Zone". In Zone IV, all components are carried away by the fresh solid inlet to ensure clean desorbent can be recycled, and therefore, Zone IV is also called the "Buffer Zone".

A detailed explanation of the movement direction of components is given here. All components in the liquid phase move counter-clockwise, and all components adsorbed to the adsorbent move clockwise. The overall direction of the movement of each component is

determined by (a) the strength of the adsorption and (b) the speed of the liquid movement, and (c) the speed of the solid movement. In TMB, the movement speed for the solid phase is the same in all zones. Zone I usually has the highest liquid flow rate, and both of the heavy and lighter components move towards the extract port. Zone II has lower flow rates compared to Zone I because of the extract flow. In Zone II and Zone III, the heavy components move towards the extract port – the direction dominated by the solid movement, and the lighter components move towards the raffinate port – the direction dominated by the liquid flow. Zone IV usually has the lowest liquid flow rate, and all components move towards the raffinate port.

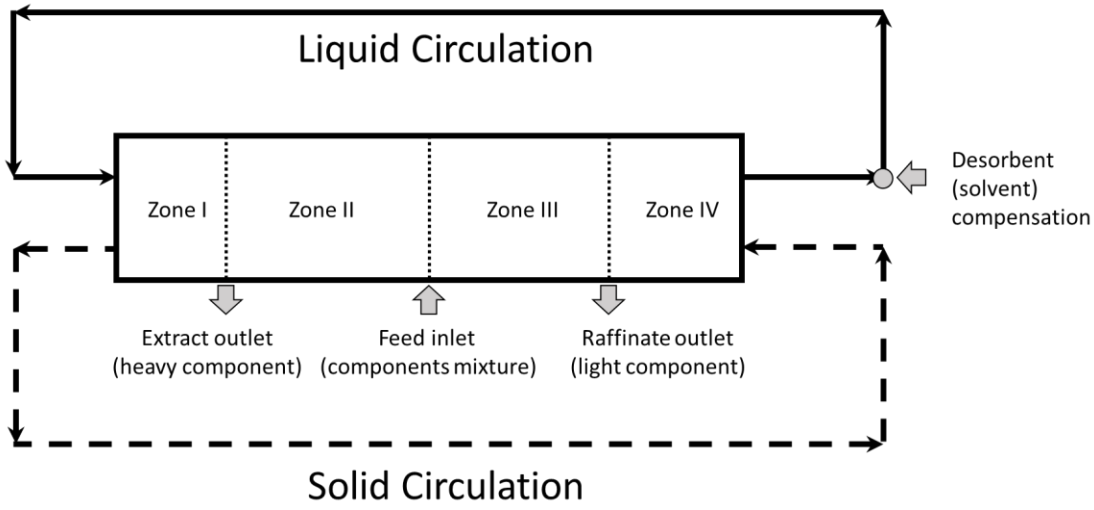

Figure 1 – A schematic of the True Moving Bed (TMB).

The movement direction of the components can be analyzed using the dimensionless flow rate ratio m_j [18]. Equation 1 shows the definition of the dimensionless flow rate ratio, where $\dot{V}_{j,TMB}$ is the liquid flow rate of zone j, $\dot{V}_{ads}$ is the solid flow rate, and ε is the void fraction of the column.

$$m_j = \frac{\dot{V}_{j,TMB} - \dot{V}_{ads}\varepsilon}{\dot{V}_{ads}(1-\varepsilon)} \quad (1)$$

When the adsorption equilibrium is described by the linear isotherm (Henry's law), the following guideline for complete separation can be used (Equation 2-5). Here, H_A and H_B are the Henry's constant for component A and B, where component A is the heavier component.

Zone I: $m_I \geq H_B, m_I \geq H_A$ (2)

Zone II: $H_A \geq m_{II} \geq H_B$ (3)

Zone III: $H_A \geq m_{III} \geq H_B$ (4)

Zone IV: $m_{IV} \leq H_B, m_{IV} \leq H_A$ (5)

1.2.2 Simulated Moving Bed (SMB) Processes

The TMB system provides a clear physical understanding of the counter-current separation; however, the TMB processes cannot be built easily. To realize this concept, SMB processes were developed which utilize column switching to simulate the movement of the solid phase.

Figure 2a shows a schematic of a 4-zone, 16-column SMB system. There are two inlets, feed and desorbent, and two outlets, extract and raffinate, as shown in this figure. Zones are defined based on the positions of inlets/outlets locations. Figure 1a shows the allocation of columns into 4 zones. For example, zone 1 is between the desorbent inlet and the extract outlet

whereas zone 2 is between the extract and the feed. The SMB operation can be illustrated as follows: all the inlet/outlet streams move one column downstream at a fixed time interval (a step time) while maintaining their relative positions. For example in Figure 1a, desorbent is supplied to column 1, the feed is supplied to column 10, the extract is withdrawn from column 5, and the raffinate is withdrawn from column 13. In the next step (Figure 2b) all inlet/outlet positions move one column downstream. i.e., to columns 2, 11, 6, and 14 respectively.

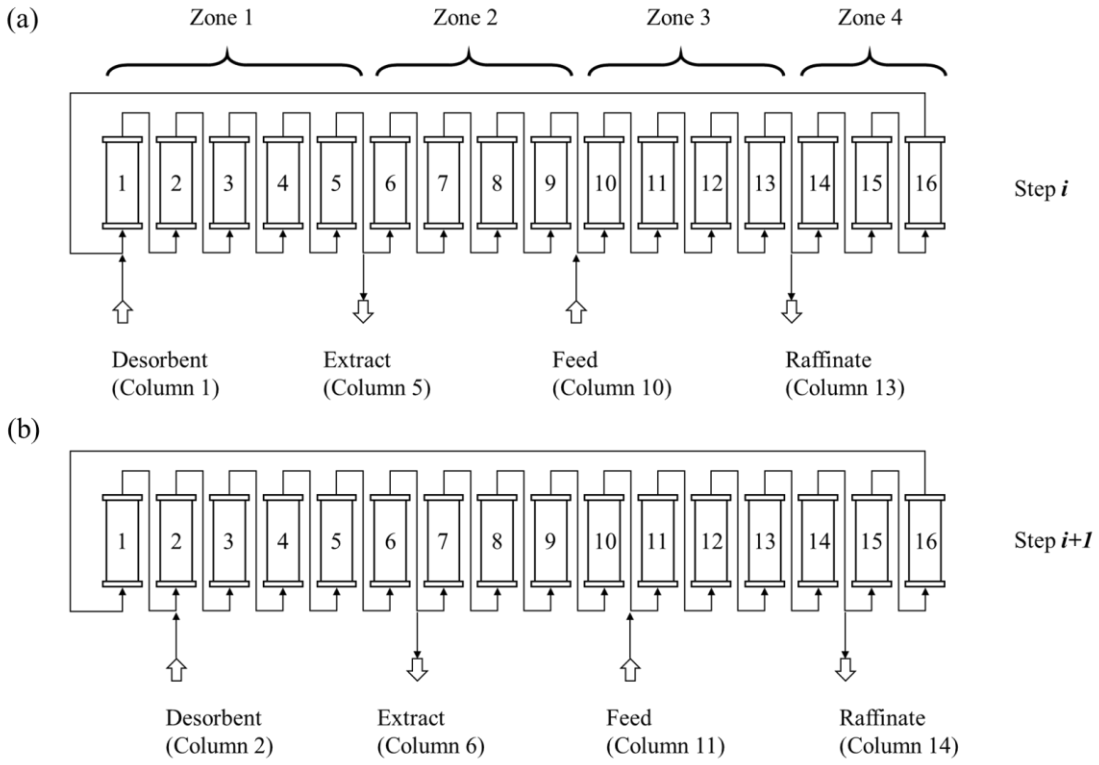

Figure 2 – 16 Column SMB schematic.

Similarly to the TMB processes, the dimensionless flow rate ratio can also be defined for the SMB processes. Here, $F_{j,SMB}$ is the flow rate in zone j, and V_{col} is the column volume. For a complete separation of a two-component system under linear adsorption isotherm, the same separation guidelines apply (Equation 2-5) using the following definition of the dimensionless flow rate:

$$m_j = \frac{F_{j,SMB} - V_{col}\varepsilon}{V_{col}(1-\varepsilon)} \quad (6)$$

The main difference between SMB and TMB is that TMB has steady-state while SMB has cyclic steady-state (CSS). In CSS, the control variables (flow rates, etc.) and the process state variables (concentrations, etc.) change periodically, and these variables return to the same values at the beginning of one period. In SMB, all of the purity, recovery as well as the internal concentration profiles have temporal variations. Depending on the type of operation, the SMB processes can be stepwise symmetric or cyclic symmetric. The illustration given in Figure 2 is an SMB operate in a stepwise symmetric manner, where every step is the same. However, each step can be operated differently from one another, while identical cycles that consist of the same set of steps are repeated. It is reported that such complex operations can be explored to achieve superior separation performance [19, 20].

1.3 **Optimization of SMB processes**

1.3.1 Region of Separations

SMB processes can be optimized to achieve the highest possible productivity while satisfying purity and recovery constraints. A triangle diagram can be plotted where m_{III} is plotted against m_{II} to find and visualize the optimal operation [15]. Figure 3 shows a triangle diagram for SMB separation of components with a linear adsorption isotherm. Here, the region for complete separation is a right triangle (a graphical representation of Equation 2-5), and the right angle point (point ***O***) of the triangle is the optimal point for separation. The region that is directly above the triangle region achieves pure extract for the heavy component but impure raffinate. The

region to the left of the triangle region gives pure raffinate product but impure extract product. Other areas lead to impure products for both extract and raffinate.

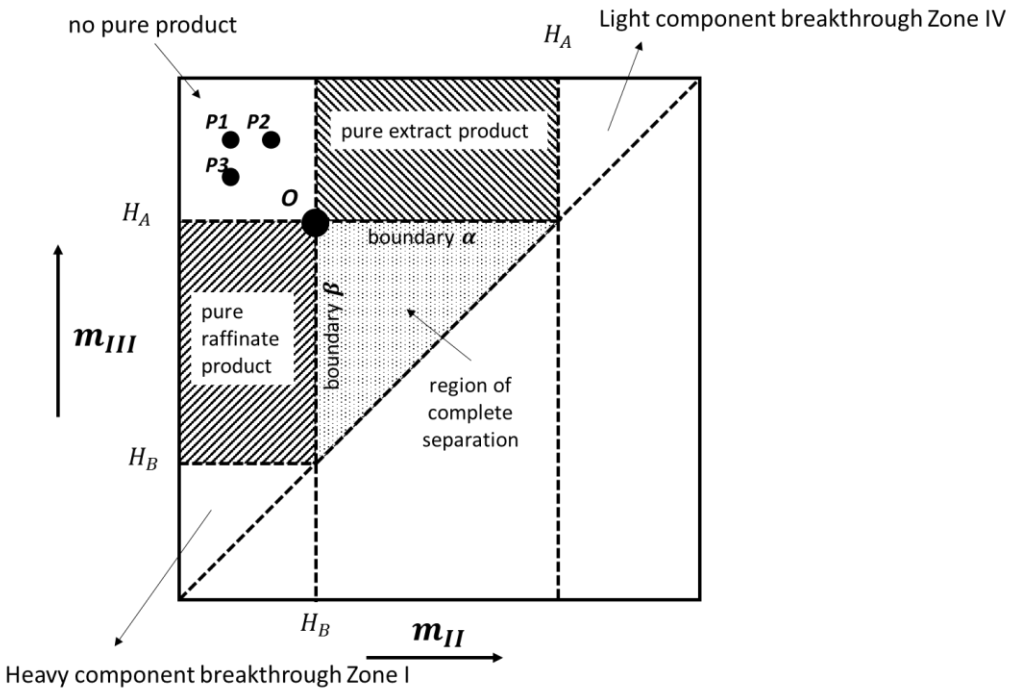

Figure 3 – Triangle diagram for linear isotherm.

1.3.2 SMB Optimization with Nonlinear Isotherm

The region of separation may have a twisted shape if the adsorption isotherm is not linear, but the concepts remain the same [21-24]; for SMBs with nonlinear adsorption isotherms, a similar design method exists, which is discussed below. When comparing operating condition points plotted on m_{III} vs m_{II} plane, a few general trend can be summarized. If the operating condition plotted (point ***P2***) is on the right of the previous operating condition (point ***P1***), an increase of extract purity can be observed. Similarly, if the operating condition plotted (point ***P3***) is directly below the previous operating condition (point ***P1***), an increase of raffinate purity can be observed. However, these trend is only true when the recycle stream of the desorbent is clean.

If the recycle stream is contaminated, then impure products may be found in both extract and raffinate streams.

There are similar analytical methods for finding the optimal SMB operating conditions with nonlinear and competitive isotherm [21, 23, 25]. In case of nonlinear isotherm, boundary $\boldsymbol{\alpha}$ and $\boldsymbol{\beta}$ are curves instead of being straight lines, and the intersection between boundary $\boldsymbol{\alpha}$ and $\boldsymbol{\beta}$, point $\boldsymbol{O}$, is still the point for maximum productivity. These analytical calculations become more difficult with respect to the increase of system complexity.

1.4 **Modeling of SMB processes**

1.4.1 SMB Model Assumptions

A large-scale nonlinear programming approach [26, 27] to model and to optimize the SMB operation numerically is described here. The SMB models are usually formulated under a few assumptions. The five assumptions given below were followed by explanations and justifications with published literature reports.

1. Mass transfer between the liquid phase and the solid phase is dominated by pore diffusion (please see Figure 4) and can be modeled by linear driving force (LDF) model.
2. All columns have the same overall porosity.
3. Liquid flow inside of the columns is equally distributed, and there is no concentration gradient in the radial direction of the column.
4. Dead volumes within or between columns are symmetric throughout the entire system to ensure step-wise symmetry.

5. There is no significant secondary retention mechanism.

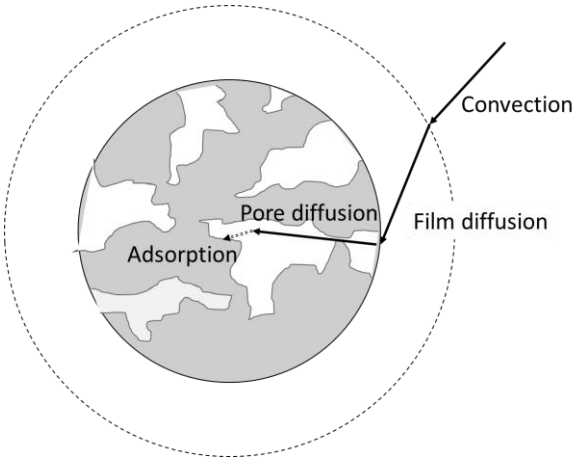

Figure 4 – Mass transfer process from bulk mobile phase to stationary phase.

The correctness of assumption 1 requires an analysis of the mass transfer process from the liquid phase to the solid phase. Mass transfer from the bulk liquid phase to the adsorption site include roughly four steps: convection, film diffusion, pore diffusion and adsorption. Convection and adsorption processes are usually very fast [28, 29]. For preparative chromatography, the particle size is usually large enough so that the transport resistance in the pore is the dominant contribution [30]. In this case, Glueckauf and Coates proposed a linear driving force model in the solid phase to describe the mass transfer in the solid [31].

Other assumptions also should also be considered carefully to ensure a good match between the model prediction and experimental results. For example, close attention should be paid to columns and frits used in the column end fittings to make sure assumptions 2 and 3 in the model are true. Dead volumes in the experiments should also be treated carefully. Dead volumes can be the headspace at the entrance of each column, the tubing volumes between every two connected columns. The size of these volumes need to be made the same in each column (i.e.,

symmetric) to ensure the delay of the liquid movement in each step is the same, and therefore the assumption 4 can hold true.

1.4.2 SMB Modeling

Over the last few decades, the design of chemical processes has been modernized with the aid of systematic numerical solution techniques [32]. The design of thermal/temperature swing adsorption (TSA) processes, pressure swing adsorption (PSA) processes, simulated moving bed (SMB) processes and many other separation processes are often carried out with some mathematical models to consider convection, mass transfer, and adsorption thermodynamics [33] [34]. These mathematical models can be solved numerically to predict process performance before carrying out validation using pilot plants.

Mass balance involves convection, diffusion, and interphase (liquid-solid) mass transfer is usually used in SMB modeling. The mass balance equation (equation 7) describes the change of bulk liquid concentration at a specific position inside of a column concerning dispersion, convection, and adsorption/desorption process. Here, $C_{i,n}(z,t)$ is the liquid phase concentration at axial location z and time t for component i of column n, and $q_{i,n}(x,t)$ is the adsorbate concentration; $\mathcal{D}_L(t)$ is the dispersion coefficient and $v_j^*(t)$ is the interstitial velocity.

$$\frac{\partial C_{i,n}(z,t)}{\partial t} = \mathcal{D}_L(t)\frac{\partial^2 C_{i,n}(z,t)}{\partial z^2} - v_j^*(t)\frac{\partial C_{i,n}(z,t)}{\partial z} - \frac{(1-\varepsilon)}{\varepsilon}\frac{\partial q_{i,n}(z,t)}{\partial t} \qquad (7)$$

The LDF model is shown in equation 8. This equation describes the mass flux into the solid phase, which is driven by the difference between the adsorbate concentration at the equilibrium, $q_{i,n}^{eq}(x,t)$, and the actual adsorbate concentration, $q_{i,n}(x,t)$. The adsorbate

concentration at the equilibrium could be calculated by one of the isotherms discussed above given the corresponding parameter.

$$\frac{\partial q_{i,n}(z,t)}{\partial t} = k_{ma}\left(q_{i,n}^{eq}(z,t) - q_{i,n}(z,t)\right) \tag{8}$$

Here, k_{ma} is the mass transfer coefficients which usually depends on the effective diffusivity of the pore diffusion process, which is correlated to the bulk diffusivity, pore porosity, constructivity (ratio of the diameters between the diffusion particle and the pore), and tortuosity (the structure and shape of the pores). The bulk diffusion for components that have nearly the same size is similar according to the Stokes-Einstein equation:

$$D = \frac{RT}{N_A}\frac{1}{6\pi\eta r} \tag{9}$$

where R is the gas constant, T is temperature in Kelvin scale, N_A is the Avogadro number, η is the viscosity and r is the particle radius. Therefore, it is convenient and correct to use the same mass transfer coefficient value, k_{ma}, for similar components in a mixture.

The model should be also constrained to satisfy cyclic steady state condition equations 10 and 11. The cyclic steady state describes a stepwise symmetric SMB operation where the liquid concentration $C_{i,n}(x,0)$ and adsorbate concentration $q_{i,n}(x,0)$ for column n at the beginning of a step ($t = 0$) are the same as those in column $n+1$ at the end of the step ($t = t_{step}$).

$$C_{i,n}(x,0) = C_{i,n+1}(x,t_{step}) \tag{10}$$

$$q_{i,n}(x, 0) = q_{i,n+1}(x, t_{step}) \tag{11}$$

1.4.3 Formulation of nonlinear programming problem for SMB optimization

The SMB processes can be modeled as nonlinear programming (NLP) problem for process optimization. The objective function (equation 12) is maximizing the feed flow rate (productivity), where the main performance constraints are the purity and recovery of the extract product (equations 13 and 14). This nonlinear problem also includes other process models (mass balances, CSS, etc.) as equality constraints (Equation 7, 8, 10, and 11).

$$Maximize\ \varphi = F_{Fd} \tag{12}$$

$$Pur_{Ex} \geq process\ performance\ specification \tag{13}$$

$$Rec_{Ex} \geq process\ performance\ specification \tag{14}$$

Other than the purity and recovery constraints given above as examples, the flow rates, desorbent-to-feed ratio, and many other SMB operating parameters can all be implemented as inequality constraints in this nonlinear programming problem. The inequality constraints and the objective function are also interchangeable. For example, instead of maximizing productivity as is shown above, the minimum productivity can be set as a constraint, and the purity can be maximized. There are trade-offs between the objective function and inequality constraints. For example, productivity can be sacrificed for higher product purity. There could be trade-offs

among inequality constraints if the productivity were to be maintained. For example, less desorbent can be used for the same productivity if purity requirement is lowered.

Decision variables in the NLP can be categorized into state variables or control variables. In our problem, state variables are mobile phase concentrations and solid phase concentrations. The value of these variables depends on the choice of control variables: the flow rates and the switching time. All flow rate variables in the model have lower and upper bounds. These restrictions are usually translated into inequality constraints in nonlinear programming problems. Most of those constraints remain *inactive* in the final solution, where the final values for the flow rates do not equal to their low or upper bounds. Therefore, the optimal solution to the NLP is not limited by the system design. Sometimes, however, the SMB system design cannot handle a very high flow rate. In these cases, some flow rates (usually Zone I flow rate) would reach the upper bounds, and the corresponding flow rate constraints become active.

The NLP problem can be solved using a nonlinear solver. In general, a nonlinear solver requires the calculation of the derivatives of each decision variables. Therefore, the functions related to these decision variables should be continuous and smooth enough within the domain of calculation. Details related to the solution of NLPs are not a focus of this thesis and can be found elsewhere [35].

CHAPTER 2. THE RATIONALE FOR A CONCURRENT APPROACH

Formulating the adsorption isotherm accurately through the efficient planning of the experimental study is of the paramount importance since the accuracy of the model prediction depends on the accuracy of the isotherm model. There are two main approaches to study and formulate the adsorption isotherm experimentally. One approach involves the studying of the adsorption of single component adsorption and combing the single component adsorption isotherm to generate a multicomponent isotherm. The other approach involves studying the multicomponent adsorption behavior and formulating the multicomponent adsorption isotherm directly. Both of the two approaches have their advantages and disadvantages. I proposed another approach – the concurrent approach – where I aim to combine the advantages of both of the two traditional approaches.

2.1.1 Multicomponent Isotherm Based on Single Component Adsorption

One commonly used approach is to study single component adsorption isotherm first, and then the single component isotherm parameters are then extended to the corresponding multicomponent isotherm. This idea behind this approach originated from the development of multicomponent Langmuir isotherm.

Butler and Ockren pioneered the idea of multicomponent Langmuir isotherm [36]. They derived the equation for the simultaneous adsorption of two solutes based on Gibb's equation. Equations 15 and 16 are the original formula of the binary mixture Langmuir isotherm developed by Butler and Ockren, where Γ_1 and Γ_2 are surface concentration of the adsorbates, c_1 and c_2 are

liquid phase concentration, A_1 and A_2 are areas can be occupied by a single adsorbed molecule, and k_1, k_2 are constants. The multicomponent Langmuir isotherm was widely used since then.

$$\Gamma_1 = \frac{c_1}{k_1 + \frac{k_1}{k_2} A_2 c_2 + A_1 c_1} \tag{15}$$

$$\Gamma_2 = \frac{c_2}{k_2 + \frac{k_2}{k_1} A_1 c_1 + A_2 c_2} \tag{16}$$

Choy et al. studied the adsorption of three acidic dyestuffs and compared experimental data with the model. However, a significant mismatch was found for binary adsorption system of Acid Blue (AB80) and Acid Red (AC114), and they proposed a modified multicomponent Langmuir isotherm to improve the fitting quality [37].

In addition to the multicomponent Langmuir isotherm which is used commonly, there are many other isotherms, including Sips isotherm [38], multicomponent Langmuir Freundlich model [39], multicomponent fowler isotherm [40], etc. Applicability of these isotherms are specific to applications, and a universal theory or isotherm that can apply to all systems does not exist.

It is often hard to find one isotherm to describe complicated adsorption phenomena. Tournier et al. studied the adsorption equilibrium of xylene isomers on BaX zeolite. There were three different components in their system: *p*-xylene, *m*-xylene, and para-diethyl benzene. In their work, single component adsorption data were collected first, and a Langmuir-Freundlich-type isotherm was found to be the best fit for multicomponent adsorption. However, there was a

significant mismatch between experimental values and calculated values for equimolar *m*-xylene/*p*-diethyl benzene mixture at 130 ^{o}C [39].

In general, the advantage of combining single component isotherm for multicomponent isotherm is the modest experimental effort. In this approach, only single component adsorption experiments are needed, which are easier to carry out. The disadvantages are the accuracy of the fitting may be unsatisfactory. As Tournier et al. and Choy et al. have both found out, the multicomponent adsorption isotherm based on single component adsorption was not always accurate.

2.1.2 Direct Study of Multicomponent Adsorption

Adsorption under competitive condition can be measured directly using multicomponent mixtures. In this approach, multicomponent adsorption experiments are conducted, the isotherm models are experimentally parameterized. In this approach, attention needs to be paid to design experiments.

To design experiments, full factorial design can be used. Talu and Zwiebel studied the multicomponent adsorption of H_2S, CO_2, C_3H_8 mixture on H-mordenite molecular sieves [41]. Their design of experiments can be described as follows: a series of experiments was run at various gas pressures with a fixed gas composition of an equimolar mixture of the three components, and a series of experiments of several mixture compositions were run at a fixed total pressure of 13.35 kPa. In this approach, all components were given the same importance in the design space; this approach can be considered as a full-factorial design.

The number of experiments required in the full factorial design can be astronomical. The following equation shows the equation for the number of experiments in a full factorial design,

$$N^{EXP} = NL^{NF} \tag{17}$$

where N^{EXP} is the number of experiments, NF is the number of factors, which equals to the number of competing species, and NL is the number of levels, which equals to how many different concentrations should be studied per component. For example, if there are five components, and for each component concentrations are divided into 10 levels, then 100000 experiments must be carried out to complete a full factorial design. In general, the advantages of this approach is that multicomponent adsorption is studied directly. However, the disadvantages include the significant experimental effort.

Moreover, multicomponent adsorption experiments are more complicated to conduct [42]. Experimental methods of obtaining adsorption isotherms include batch experiments and chromatographic pulse tests. Analysis of such tests can be performed by moment analysis, frontal analysis, the perturbation method, the inverse method, etc. [15]. Depending on the separation system, the difficulty of conducting these experiments may vary. Most adsorbent characterization methods for single or binary adsorption system cannot be readily applied to multicomponent adsorption system. For example, UV-Vis/Refractive Index Detector (RID) which were often used in breakthrough experiments usually cannot distinguish more than two components simultaneously. For some systems, common optical detectors may be not sensitive enough to distinguish similar compounds, such as structural isomers.

Some experimental approaches have been developed to address this challenge. Tournier et al. developed two methods of detecting physically similar components [42]. One method involves using a carbon isotope to mark each different component and send column eluent to a furnace and then a mass spectroscopy to examine the abundance of each component. Another method involves an offline gas chromatography analysis as the second step to analyze the sample. Minceva and Rodrigues reported a study of xylene adsorption on a faujasite zeolite by batch experiments [38]. A batch that contains adsorbents and adsorbates was pressurized to 9 bar in helium and heated to 180 ^{o}C to mimic the realistic conditions in industrial adsorption processes. To deal with the high temperature and pressure, a sampling valve to a gas chromatography was used to automate the sampling procedure. However, none of the aforementioned experimental methods allow the analysis of multiple samples simultaneously, and the analysis of each individual sample is still time-consuming.

2.1.3 The Concurrent Approach

In the concurrent approach, multicomponent adsorption experiments are carried out to provide a direct assessment of the adsorption behavior under component competition. To reduce the experimental efforts, the experimental conditions are to be selected based a prediction of the optimal operating condition of the process to be designed. Model simulations and optimizations are carried out to assist the prediction of the optimal operating condition of the process.

Many process models employ Henry's law or Langmuir isotherm to avoid complex numerical calculation. When a simple isotherm is applied to a complex multicomponent adsorption system, interactions among components may be oversimplified, and the numerical prediction may only be accurate within a narrow range of concentrations and compositions. It

should be noted, however, that no practical separation process operates at the entire range of possible liquid compositions. It is possible to model the adsorption in a small range of liquid compositions, namely, a local model. Therefore, it is possible for the local model to take on a simple numerical structure.

In this thesis, I propose a model-based, iterative, concurrent approach. The testing of the isotherm does not include all possible combinations of components; instead, a process model predicts possible compositions in the mobile phase of an adsorptive separation process (a model-based design). The initial model simulation and optimization are based on the rough estimation of the isotherm parameters obtained from preliminary experiments or from literature reports. Then, the model parameters are updated with experimental data (an iterative method). Each iteration can lead to more accurate and reliable model prediction; and in the final iteration, an optimal operation, as well as a set of isotherm parameters, can be obtained simultaneously (a concurrent approach).

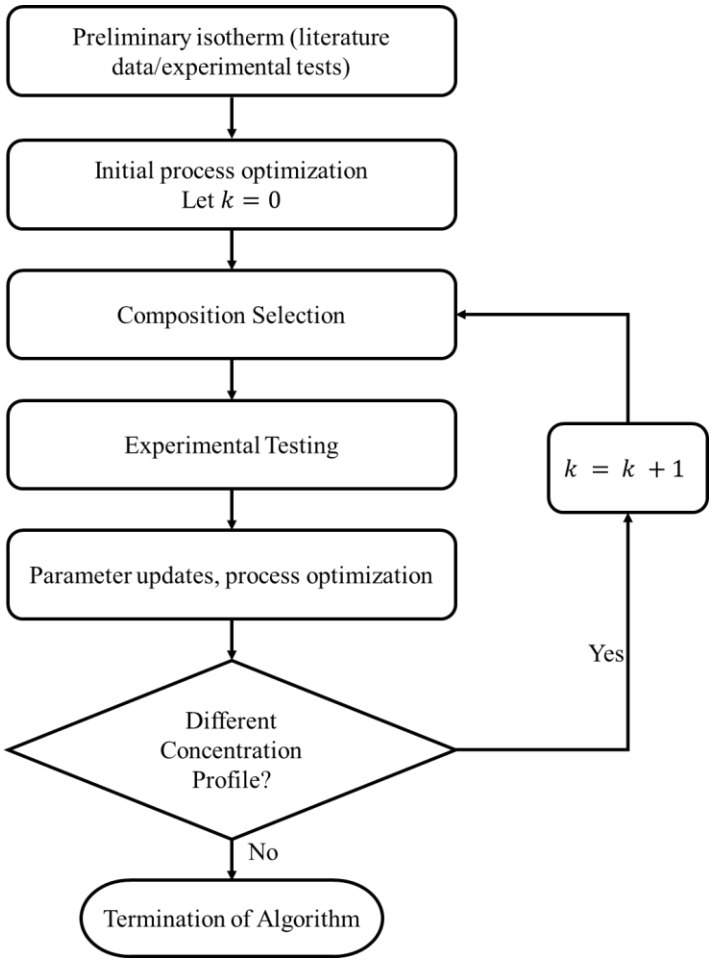

Figure 5 - Illustration of the iterative approach of finding SMB optimal operating condition while developing adsorption isotherm.

In order to find a local model, the internal concentration profile must be predicted; however, the prediction of the internal concentration profile by a mathematical model can be accurate only if an accurate isotherm model is available. Therefore, an iterative-concurrent approach was proposed to find the optimal operating conditions for the separation process simultaneously while developing the multicomponent adsorption isotherm. Figure 5 outlines the proposed iterative and concurrent approach. The method starts with process simulation and optimization with preliminary isotherm parameters, which can be obtained from the literature. If such information is not available in the literature, this initial guess can also be generated by a few

preliminary experimental measurements. Next, representative compositions are selected from the internal concentration predicted by a process model. The algorithm for composition selection is described in a later chapter (Chapter 3). In the following step, experimental measurements are carried out at these different compositions. For example, these selected compositions can be used as feed compositions in breakthrough experiments or initial compositions in perturbation experiments. In this report, breakthrough experiments were used, and the concurrent approach is illustrated in details in later sections. After carrying out experimental measurements, adsorption data is used for updating isotherm parameters, and the process optimization is carried out again in the next iteration. By repeating the steps discussed above, it is assumed that the isotherm parameters and the optimal design of the adsorption process converge. After the convergence, there is no more significant change in internal concentration profile, and thus the method can be terminated. This method yields the optimal operating conditions for an isotherm validated at the compositions in the process.

CHAPTER 3. A CONCURRENT APPROACH FOR PROCESS DESIGN AND MULTICOMPONENT ADSORPTION MODELING WITH LOCAL ISOTHERMS

3.1 Motivation

There are two main challenges that make the design of multicomponent adsorptive separation process difficult: (a) the significant experimental effort and (b) the lack of an accurate but simple adsorption isotherm. I am motivated to streamline the process development by proposing a concurrent, model-based process development approach that improves model prediction and reduces experimental effort. The target systems of applying this approach are separation processes that involve multicomponent adsorption.

3.1.1 Challenge (a): Experimental Effort for Multicomponent Isotherms

Adsorption isotherms are physical, empirical, or statistical models that describe the equilibrium of adsorption. When the adsorbate concentration can be described explicitly by the mobile phase concentration, the isotherm model is usually in the form:

$$q_i^{eq} = f(C_i) \tag{18}$$

where i is the index for component in the system, q_i^{eq} is the equilibrium adsorbate concentration, C_i is the mobile phase concentration, and f is a function (adsorption model) that establishes the relation between q_i^{eq} and C_i.

Establishing such an adsorption model for a single component system is significantly simpler than obtaining a multi-component isotherm. Experimentally, the equilibrium adsorbate concentration, q_i^{eq}, can be measured at each different liquid phase concentration, C_i. Therefore, an adsorption model can be found by testing the adsorption at multiple liquid phase concentrations, C_i. However, the conventional approach becomes inefficient and ineffective when competition among components cannot be ignored, and the isotherm model needs to consider the component interactions. Such a system can be modeled by an isotherm in the following form:

$$q_i^{eq} = f_i(C_1, C_2, .., C_{NComp}) \tag{19}$$

where f_i is the adsorption isotherm model that establishes the relation between q_i^{eq} and all the possible C_i's, and N_{Comp} is the total number of components in the multicomponent adsorption system. In a traditional combinatorial approach, not only the single component adsorption needs to be measured, but the binary (n = 2), ternary (n = 3), and more complex interactions of components need to be investigated thoroughly as well. The complexity of the adsorption model usually increases with the increase of the number of components. Therefore, obtaining detailed multicomponent adsorption information can be extremely demanding. Hundreds of samples may need to be tested in order to study the adsorption systematically.

3.1.2 Challenge (b): Lack of General Adsorption Isotherm

The multicomponent adsorption mechanism is usually very complicated and not fully understood. For example, the adsorption of xylene on molecular sieves is still not fully understood despite several decades of industrial practice. A few mechanisms of xylene adsorption on zeolite that are not fully understood include: (1) adsorbate loading becomes stepwise at some

temperatures [43], (2) the adsorption is affected by both heat of adsorption and pore volume [44], (3) the selectivity of *p*-xylene is enhanced at lower water loading, but suppressed at higher water loading [40], (4) selectivity of *p*-xylene is affected by adsorbate loading and also adsorbate composition [45]. Most studies attribute these unique features to the combination of entropic and energetic effects. There are not any adsorption models that can be readily used to match all those observations or a theory that can unify all potential mechanisms in xylene adsorption.

The complex nature of the multicomponent adsorption calls for a systematic study. There have been many attempts to model xylene adsorption isotherms on zeolite [38, 39, 46, 47]. Many isotherm parameters given in literature can match experimental observations qualitatively, but I am not aware of an isotherm that provides sufficient accuracy for process model simulation and optimization. Some of these studies emphasize the adsorption of single component or did not include all of the five main components (*p*-xylene (PX), *m*-xylene (MX), *o*-xylene (OX), ethylbenzene (EB) and *p*-diethyl benzene (PDEB)) in multicomponent adsorption experiments, and hence the prediction of adsorption under competition is unwarranted. Some of these studies were not carried out at or near the saturation conditions in industrial processes, and thus the adsorption data cannot be used to predict separation performance.

One of the most commonly used isotherms for the xylene separation process model is the extended-Langmuir isotherm:

$$q_i^{eq} = \frac{H_i C_i}{1 + \sum_{j=1}^{NComp} b_j C_j} \tag{20}$$

This simple isotherm is based on several assumptions that include (1) identical adsorption sites for all species and (2) no component interactions. For multicomponent xylene adsorption on

molecular sieves, both of the two assumptions may not be valid: Mellot et al. found that when there is more than one molecule adsorbed per α-cage, the second molecule forces the first molecule to reorient together with the second molecule and form π–π interaction to stabilize the adsorption[48]; Lachet et al. proposed that there are four different sites for xylene adsorption on zeolites, "II/III", "II", "II/W" and "W", and each has a different adsorption energy for each different xylene isomers [44]; Pichon et al. studied the location of *p*-xylene adsorption on pre-hydrated zeolites, and found that there are two different adsorption sites in the α-cage that adsorb *p*-xylene and on average about 3.3 *p*-xylene molecules can be adsorbed per α-cage [49]. Some empirical modifications can be applied to the Langmuir isotherm structure to fit experimental data, but only "qualitative results" were obtained [39].

Other approaches such as the ideal adsorbed solution theory (IAST), the real adsorption solution theory (RAST), the vacancy solution theory (VST) and the potential theory of adsorption (PTA) have been proposed to address the deficiency of the extended-Langmuir isotherm. One of the most studied approaches is the IAST. It is often considered to be more versatile than extended-Langmuir isotherm, but it is significantly more computationally expensive making it less suitable for process modeling and optimization without special numerical treatments [50]. The IAST also relies on accurate single component adsorption data within Henry's region (infinite diluted solution), the inaccurate measurement of which may lead to poor evaluation of multicomponent equilibria [51]. Moreover, when the saturation capacities of different species are similar to each other, the equilibrium described by the IAST reduces to the extended-Langmuir isotherm, and this approach is no longer advantageous over the simple extended-Langmuir isotherm.[52].

This article is organized as follows: several existing challenges for designing separation processes involving multicomponent adsorption are discussed. The proposed approach to address

these challenges is described in the section 3.1.1 and 3.1.2, and an example is followed to illustrate the proposed approach. The detailed methodology of mathematical modeling and experimental set-up is included in section 3.3. The results section shows the convergence of the approach and the accuracy of a local model, as well as the sensitivity analysis with respect to uncertain model parameters and variations in process design.

3.1.3 Example: Xylene Adsorption on Zeolite by SMB

Currently, the majority of PX is produced by SMB processes such as UOP's Parex, IFP's Eluxyl, and Toray's Aromax. In UOP's Parex process, there are 24 adsorption columns connected to a 24-port rotary valve. Other than the four main inlets/outlets, there are also a few flushing streams that are used to clean up the transfer lines [53].

In this report, xylene separation by the SMB process is studied as an illustration of the proposed concurrent process design and isotherm measurement approach. In this study, flushing streams, as well as the effect of impurities in the feed (toluene and non-aromatics), were ignored. A 24-column SMB for xylene separation of the industrial scale was assumed and modeled.

Xylene adsorption on zeolites is well-known because of its application in the industrial separation process. This is a challenging system that has at least five components: PX, MX, OX, EB, and PDEB. The first four components are present in the typical mixed xylene feedstocks, and the fifth component, PDEB is the desorbent used to elute and separate xylene mixture. Toluene and non-aromatic species may also be present in the system and affect the separation. As there are five main components, a factorial design may include many experiments for non-dilute (saturated) xylene mixture. The goal of this report, however, is not to clarify the adsorption

mechanism of xylene mixture on zeolite, but to find a working isotherm for the purpose of modeling the SMB, regardless of the adsorption mechanism.

It is worth noting that the proposed concurrent approach is not limited to xylene adsorption on zeolite nor to SMB processes; it can be applied to any multicomponent liquid and gas adsorption processes such as PSA and TSA.

3.2 Experimental and Modeling Methods

3.2.1 Mathematical Modeling of Xylene Separation by SMB

A rigorous SMB model was used for process simulation and optimization. A 24-column SMB process was modeled, and zone configuration was set to 6-9-6-3 [1]; i.e., there are 6, 9, 6, and 3 columns between desorbent and extract (Zone 1), extract and feed (Zone 2), feed and raffinate (Zone 3), and raffinate and desorbent (Zone 4), respectively. Purity and recovery were chosen according to industrial standards. Governing equations, objective function and the main inequality constraints of the SMB optimization model were equations 7-14. The multicomponent Langmuir isotherm (equation 20) was implemented to describe the xylene adsorption.

The nonlinear programming (NLP) problem with the set of partial differential algebraic equations (PDEAs) was implemented within the AMPL (A Mathematical Programming Language) modeling environment [54] and solved using IPOPT 3.12 [55]. A full-discretization approach [34] for optimization was adopted, where the central finite difference scheme was applied to spatial discretization (25 nodes per column) and collocation method on finite elements (4 elements per cell) was applied to temporal discretization.

3.2.2 Isotherm Parameter Updating by Least Squares Method

When new experimental data were made available, the least square fitting was performed to update the isotherm parameters. As discussed above, the local model approach is employed in this study; not all existing experimental data participate in the parameter fitting. Only the experimental data "relevant" to the new concentration profile was used in parameter fitting. The relevant data include experimental results from feed compositions that were located on or sufficiently close to the concentration profile of the optimized SMB process.

To differentiate the experimental data point that was relevant to the current concentration profile and those were not, a binary variable was defined as follows:

$$\zeta_{k,p} = \begin{cases} 1 & \exists x \in [0, L] \text{ such that } \left\| \overrightarrow{C_p} - \overrightarrow{C_k}(x) \right\| \leq \delta_k \\ 0 & \text{otherwise} \end{cases} \tag{21}$$

where $\overrightarrow{C_p}$ is a vector of internal concentrations, $\overrightarrow{C_p} = (C_{PX,p}, C_{MX,p}, C_{OX,p}, C_{EB,p}, C_{PDEB,p})$; $\overrightarrow{C_k}(x)$ is the liquid composition on the internal concentration profile at axial position x; k is the index for iterations, and p is the index for each experimental measurement. Here, δ_k is a tolerance parameter for the current iteration, k.

Furthermore, a few definitions is given here. (1) Coverage: for a given composition vector $\overrightarrow{C_k}(x)$, if there exists an experimental data point $\overrightarrow{C_p}$ that satisfies $\left\| \overrightarrow{C_p} - \overrightarrow{C_k}(x) \right\| \leq \delta_k$, it is said that the composition $\overrightarrow{C_k}(x)$ is *covered* by experimental measurements; otherwise, it is said the composition $\overrightarrow{C_k}(x)$ is *exposed* outside of experimental measurements. (2) On/Off: for a given experimental data point $\overrightarrow{C_p}$ and internal concentration profile, $\overrightarrow{C_k}(x), x \in [0, L]$, if $\left\| \overrightarrow{C_p} - \overrightarrow{C_k}(x) \right\| \leq \delta_k$ is satisfied by any value of x, it is said that the composition $\overrightarrow{C_p}$ is *on* the

concentration profile; otherwise, it is *off* the concentration profile. Using the binary variable given in equation 21, the parameter estimation problem can be formulated as follows:

$$\text{Minimize } \varphi_k^{leastSquare} = \sum_{\substack{i=1 \\ p=1}}^{\substack{N_{comp} \\ N_{exp}}} \left(\zeta_{k,m} \cdot \left(q_{i,p,model}^{eq} - q_{i,p,exp}^{eq}\right)^2\right) \tag{22}$$

$$+M_1 \sum_{i=1}^{N_{comp}} \left(\frac{H_{i,k} - H_{i,k-1}^*}{H_{i,k-1}^*}\right)^2 + M_2 \sum_{i=1}^{N_{comp}} \left(\frac{b_{i,k} - b_{i,k-1}^*}{b_{i,k-1}^*}\right)^2$$

where, $\varphi_k^{leastSquare}$ is the objective function, ζ is the binary variable for each experimental measurements, q is the adsorbed phase concentration, q^{eq} is the equilibrium adsorbed phase concentration, b is the adsorption constant in the extended-Langmuir isotherm, and H is the henry's constant, N_{COMP} is the total number of components, N_{exp} is the total number of experiments, subscript i is the index for components, subscript k is the index for iteration ($k \geq 1$), and superscript * means optimized value.

The objective function was optimized subject to the multicomponent Langmuir isotherm model (equation 20). The value of the square difference between experimental values, $q_{i,p,exp}^{eq}$, and the fitted values, $q_{i,p,model}^{eq}$, was minimized under the penalty of the regularization terms, which ensured that the obtained parameters did not deviate from the expectation to much.

The Tikhonov regularization terms $M_1 \sum_{i=1}^{N_{comp}} \left(\frac{H_{i,k} - H_{i,k-1}^*}{H_{i,k-1}^*}\right)^2$ and $M_2 \sum_{i=1}^{N_{comp}} \left(\frac{b_{i,k} - b_{i,k-1}^*}{b_{i,k-1}^*}\right)^2$ in the objective function were included to eliminate the non-uniqueness; and this technique was shown to be effective for parameter fitting [56]. The regularization was designed in such a way

that the results of the parameter fitting process would not depend on the initial guess of the decision variables while deviation from the optimized value from the last iteration is suppressed. Weighing parameters M_1 and M_2 were adjusted by trial-and-error to control deviation of isotherm parameters from the previous iteration, while maintaining sufficiently good fitting. I found in this study that the values of M_1 and M_2 are chosen in such a way that the regularization term has minimal influence on the objective function, and only serve to eliminate non-unique solutions. The typical values for M_1 and M_2 were around 10.

It should be noted that the parameter fitting approach discussed above is only for the isotherm parameters and does not include the mass transfer parameters as demonstrated using a small-scale plant in other studies [56, 57]. In the proposed concurrent process design approach, adsorption data were sampled offline in a single column experimental set-up, and the parameter estimation only focuses on adsorption equilibrium.

3.2.3 Composition Selection Algorithm and Isotherm Fitting

The selection of representative compositions is based on the algorithm shown in Figure 6. In this algorithm, all compositions were identified that appeared in the SMB concentration profiles predicted by the model but had *not* been tested experimentally previously. Compositions predicted by the model are denoted as $\overrightarrow{C_k}(x_m)$, where k is the index of the current iteration, and m is the index of spatial discretization. The compositions that have been tested by breakthrough experiments are represented by $\vec{C}_{p,\bar{k}}$, where p is the index of experimental measurements, and $\bar{k}$ is the index of iterations. At each iteration, the compositions that had been tested form a matrix A_k, which has the following structure:

$$A_k = \begin{pmatrix} C_{pX,1,1} & C_{pX,2,1} & \cdots & C_{pX,N_{EXP},k} \\ C_{mX,1,1} & C_{mX,2,1} & \cdots & C_{mX,N_{EXP},k} \\ C_{oX,1,1} & C_{oX,2,1} & \cdots & C_{oX,N_{EXP},k} \\ C_{EB,1,1} & C_{EB,2,1} & \cdots & C_{EB,N_{EXP},k} \\ C_{PDEB,1,1} & C_{PDEB,3,1} & \cdots & C_{PDEB,N_{EXP},k} \end{pmatrix} \quad (23)$$

The selection begins with the composition at the entrance of Column 1 ($m = 0$, for $x = x_m$), $\overrightarrow{C_k}(x_0)$, by calculating the difference between this composition and one existing $\vec{C}_{p,\bar{k}}$ in A_k. If $\overrightarrow{C_k}(x_m)$ is covered by at least one of $\vec{C}_{p,\bar{k}}$, namely $\exists p \in [1, \dots, N_{exp}]$ such that $\left\|\overrightarrow{C_k}(x_m) - \vec{C}_{p,\bar{k}}\right\| \leq \delta_k$ for the current iteration *k* and spatial position x_m, then move to the liquid composition of the next spatial discretization, $\overrightarrow{C_k}(x_{m+1})$. If there is significant difference, then augment the composition matrix A_k with $\overrightarrow{C_k}(x_m)$, and then move to the liquid composition of the next spatial discretization, $\overrightarrow{C_k}(x_{m+1})$. The selection ends at the composition at the end of the last column, $\overrightarrow{C_k}(L)$, where *L* is the total length of all columns.

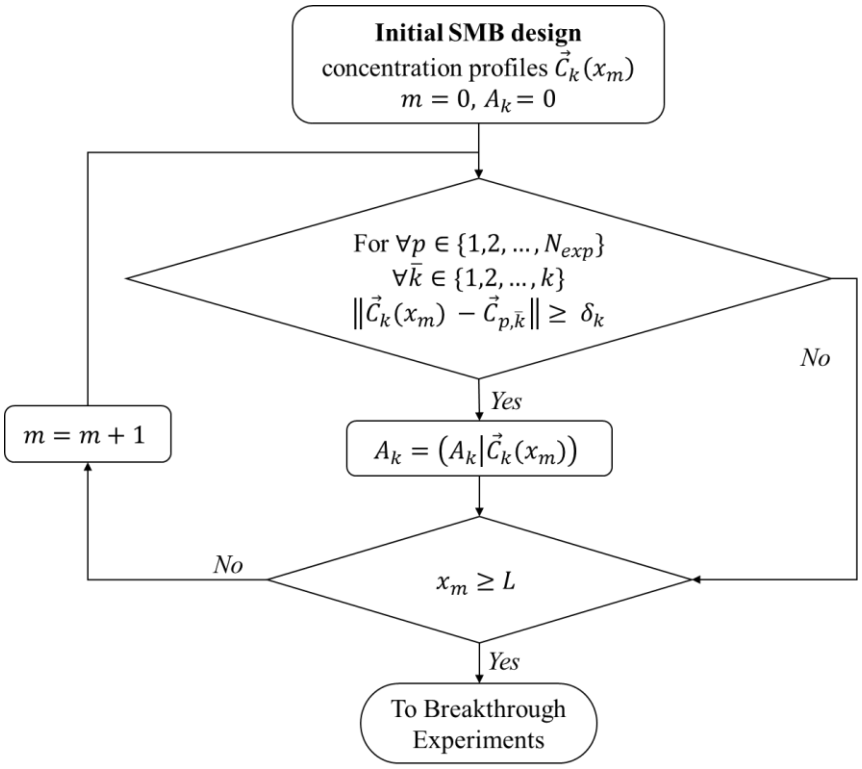

Figure 6 - Composition selection algorithm for breakthrough experiments.

An arbitrary tolerance, δ_k, was set to determine whether two compositions are sufficiently different or not. Initially this constant is set to be a large number to reduce the number of compositions selected from this algorithm. As the iterations proceed, this constant is decreased to obtain more compositions which lead to more accurate adsorption measurement. Typically, δ_k is in the range of 0.05 to 0.25 when mass fraction was used as the unit for compositions. The value of δ_k should be chosen carefully; if δ_k was chosen to be small, many liquid compositions would be chosen to be tested by experiments and fewer experimental measurements from the past would be used, and if δ_k was chosen to be too large, there was not enough experimental conditions to ensure the accuracy of the isotherm to be applied to the local composition region. The value of δ_k should be determined by trial-and-error. This approach, where differences in compositions are

measured by a vector norm $\left\|\overrightarrow{C_k}(x_m) - \vec{C}_{p,\bar{k}}\right\|$, is a systematic method that can be applied to any number of components avoiding manual or heuristic composition selection.

It should be noted that for this system, temporal changes (dynamics) of the composition are ignored since there are as many as 24 columns; with such a large number of columns, an SMB process can be approximated as a true moving bed (TMB) process, which is a steady-state process. If the proposed approach is used for an SMB with a fewer number of columns, this approximation may not be valid, and the algorithm may need to be modified.

3.2.4 Experimental Set-Up

Molecular sieves for xylene separation were prepared from generic BASF binder free 13X (13XBF) in sodium form. For each of 100 g of sieves, a 5 liter 0.2 N $Ba(NO_3)_2$ solution was used for ion-exchange. Sodium form X zeolite was suspended in the barium ion exchange solution for 1 hour at ambient temperature. Then the ion-exchanged zeolite X (BaX) was triple washed by 1 L DI water. The zeolite X was then dried overnight at 80^{o}C. The original size of the 13X beads were around 1.2 mm and were further crushed down to around 325 um (45 to 50 mesh) before packing.

The column for breakthrough experiments was 15 cm length, 1 cm ID stainless steel. The columns were assembled from Valco column end fittings and cleaned-and-capped stainless steel tubing from McMaster-Carr. After packing the column with BaX, the columns were activated under dry nitrogen flow at 200^{o}C for 12 hours to remove water. When correctly prepared, each column holds around 10.6 grams of BaX water-free adsorbent.

Guard columns were used to ensure column performance. Six columns upstream of the BaX were prepared to remove water, oxygenate, and dissolved oxygen. Three columns were used to purify desorbent, and three columns were used to purify sample mixture. Liquid flow was routed through a 15 cm length, 1 cm ID column packed with 45-50 mesh crushed 3A adsorbent and then through a 15 cm length, 1 cm ID column packed with 45-50 mesh crushed Selexsorb® CD activated alumina spheres adsorbent and then through a 15 cm length, 1 cm ID column packed with 2mm uncrushed GetterMax® 133 3x3mm/Copper type oxygen getter pellets before it entered the BaX column. Molecular sieves 3A beads were obtained from Sigma-Aldrich (02573-1kg). This adsorbent was crushed down to 45-50 mesh before packing and was activated at 200^{o}C for 12 hours before packing. GetterMax® 133 and Selexsorb® CD were both obtained from Research Catalysts, Inc. Selexsorb® adsorbent was crushed down to 45-50 mesh before packing and was activated at 200^{o}C for 12 hours before packing. GetterMax® 133 adsorbent was not crushed because of its poor stability in air, and it was activated in a 1% hydrogen/99% nitrogen gas flow at 175^{o}C for 8 hours. Guard columns were replaced every five breakthrough experiments performed (500 ~ 750 ml total solvent flow).

The breakthrough experimental setup was similar to the one in Tournier et al. [42] and Gee et al. [58]. The experimental set-up was adapted from a Shimadzu HPLC system and is shown below (Figure 7). Two LC-20 pumps were used to deliver desorbent (toluene) and sample mixture. Both of the solvents went through guard columns and then meet at the injection valve (Valco medium temperature injection valve, EH6C6WE) which can switch the mobile phase from desorbent to sample mixture. After the injection valve, a GC-8A oven was adapted to heat up the BaX column and a preheating loop (10 feet) to 180^{o}C. The preheating loop has a total dead volume of 0.15 ml. After the BaX column, the liquid flowed through a 100 psig back pressure regulator

and then was sent to a fraction collector which was adapted to hold up-to 72 GC vials. Usually, liquid flow for the breakthrough experiments was 0.5 ml/min, so a cooling bath between the column oven and the back-pressure-regulator was optional. The liquid outlet was collected for about 32 min into 54 vials (each vial holds 1ml hexane and 0.3 ml sample) and one of every three vials was sent to a Shimadzu GC 2010 plus for offline analysis.

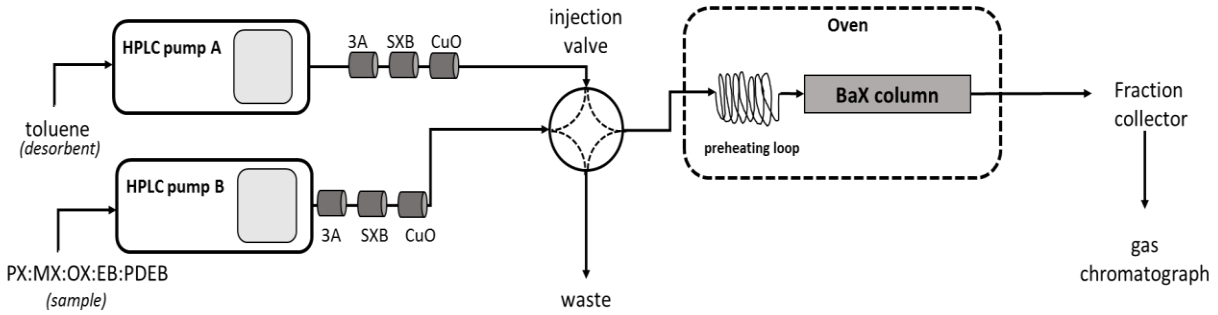

Figure 7 - Breakthrough experimental set-up

The GC column was a DB-WAXetr column from Agilent (#122-7332, 0.25mm ID, 30 m length, 0.25 um thick film, 7 in diameter loop configuration). An AOC-20i+s autoinjector/sampler was installed to the GC. Injection volume was 0.5 ul with a 10 ul syringe which was rinsed twice with hexane before and after the injection. The injector temperature was set to 250^{o}C on split mode with a split ratio of 50. The flow controller was set to maintain a linear velocity (80 kPa pressure, 55 ml/min total flow rate, 1.0 ml/min column flow rate, 25 cm/sec velocity, 3.0 ml/min purge flow rate). After the injection, the GC column was maintained at 35^{o}C for 5 min and then heated at 4^{o}C/min to 100^{o}C and then hold for 8 min. A flame ionization detector at 275^{o}C was used to detect the composition. Each sample required about 30 min to analyze to obtain good resolution between PX and MX.

Figure 8 shows a typical multicomponent breakthrough curve of mixed xylenes. The column was initially filled with toluene. The experiments were carried out at 180 ^{o}C and around 9 bar. Tri-isopropyl benzene (TIPB) was used as a tracer since it allows easier analysis for the slower evaporation rates than that of *n*-hexane or *n*-heptane. TIPB is a large and bulky molecule that should not enter the pore of the faujasite zeolite. The frontal analysis was carried out to obtain equilibrium adsorbed amount. The area between tracer and the xylene component is the amount that has been adsorbed on the zeolite. The determination of equilibrium concentrations in the adsorbent was based on mass balance as employed in Gee et al. [58].

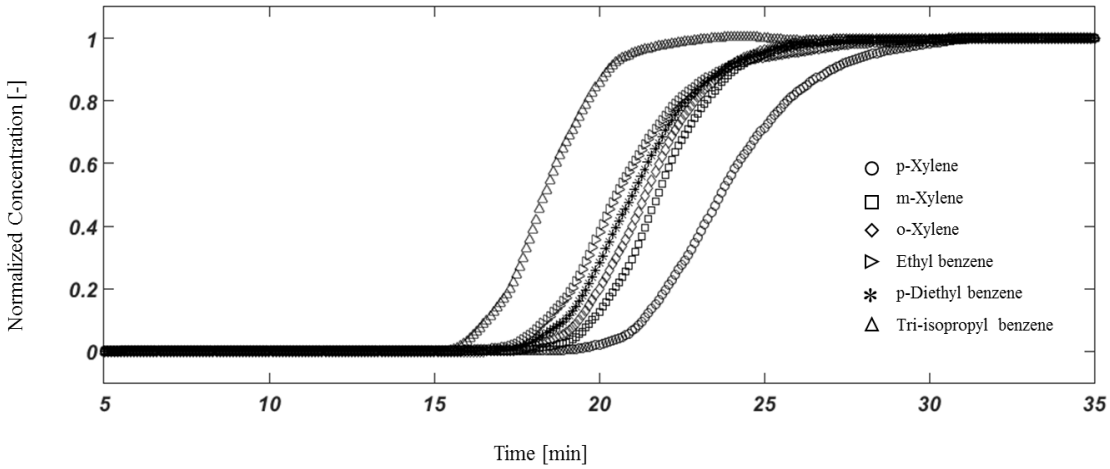

Figure 8 - A typical breakthrough curve of mixed xylenes on BaX zeolite

3.3 **Results and Discussion**

3.3.1 Iteration and Convergence

3.3.1.1 Evolution of Concentration Profile

Estimation of the concentration profile predicted by SMB process model changed after each iteration until it arrived at the final optimal result. The initial model parameters were based

on a well-known study from Minceva and Rodriguez [1], which used equilibrium data for xylene separation using potassium exchanged Y zeolite.

Figure 9 shows the evolution of the concentration profiles through the three iterations. The concentration profiles are shown in two different formats: subfigures (a), (d), (g), and (j) are the concentration profile across SMB columns where the area of each component represents their relative concentration. The vertical lines represent the compositions that were selected for breakthrough experiments. Subfigures (b), (c), (e), (f), (h), (i), (k), and (l) are the ternary composition plots of the concentrations where solid curves represent the trajectories of the concentration profiles. Solid circles on the curve represent the compositions that were selected for breakthrough experiments; dashed curves are the trajectories of the concentration profiles in the previous iterations; diamonds are compositions that have been tested previously.

Initial guess and the zeroth iteration ($k = 0$): Figure sets (a), (b) and (c) of Figure 9 show the initial guess of the concentration profile based on literature isotherm parameters. It can be observed from the SMB internal concentration profile that *p*-xylene concentrations at around $x = 0.35$ were three times higher than the feed concentration, indicating significant competition between components. This extremely strong competition may be due to overestimation of adsorption parameters, which is subject to investigation in the next iteration.

As is shown on the ternary plots (Figure 9 (b) and (c)), the SMB internal concentration profiles loop through the five-dimensional composition space as a curve instead of spanning a large region. This important feature enabled the composition selection procedure to narrow down the experimental conditions. Ten liquid compositions that were chosen to be tested are shown as vertical lines on the SMB internal concentration profiles (Figure 9(a)) and the ten solid circles on

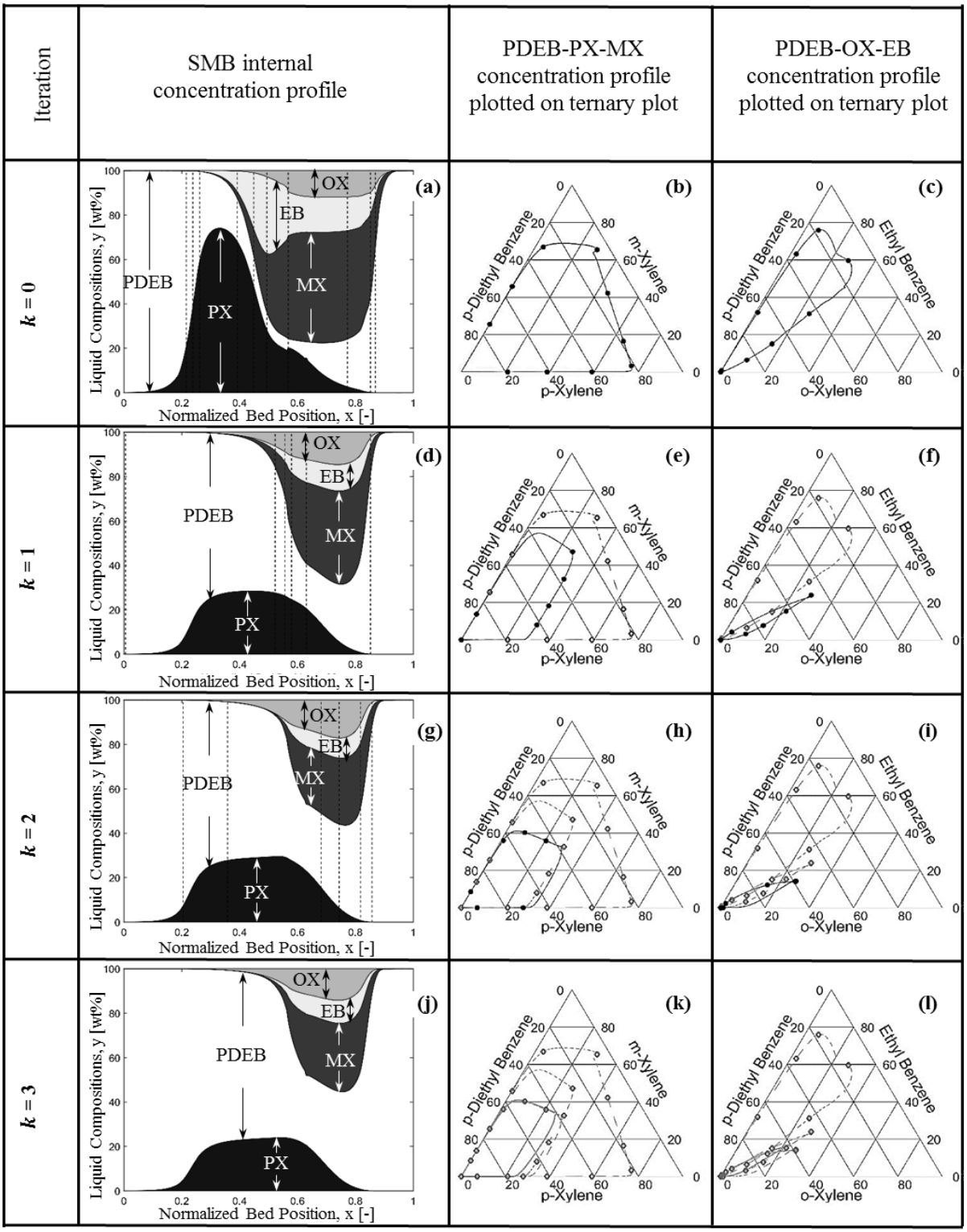

Figure 9 - Iteration history; (a), (d), (g), and (j): Internal concentration profile of the optimized SMB model in each iteration. Vertical dashed line represent the liquid compositions tested in breakthrough experiments; (b), (c), (e), (f), (h), (i), (k) and (l): ternary diagrams for selected compositions. Closed circles are the compositions tested in the current iteration, and open circles are the composition tested in prior iterations.

the ternary plots (Figure 9 (b) and (c)). The principle of choosing the ten compositions for experimental testing was designed so that the ten experimental measurements should cover the entire concentration profile as shown in Figure 6. The tolerance, δ_k, was controlled such that the required experimental measurements were not excessive. The compositions are shown in Table 2 (experiments 1 to 10), and the experimental results are shown in Table S2 in the supporting information.

Table 1 - History of isotherm parameters in iterations (initial isotherm parameters from literature report [1]). Note that Henry's constant in Langmuir isotherm is given by $\boldsymbol{H_i = b_i^{eq} Q_i^{sat} \rho_{ads}}$ where $\boldsymbol{\rho_{ads}}$ is the density of adsorbents.

	k = 0		*k = 1*		*k = 2*		*k = 3*	
Component, *i*	$b_{i,k}^{eq}$ (cm^3/g)	Q^{sat} (g/g)	$b_{i,k}^{eq}$ (cm^3/g)	Q^{sat} (g/g)	$b_{i,k}^{eq}$ (cm^3/g)	Q^{sat} (g/g)	$b_{i,k}^{eq}$ (cm^3/g)	Q^{sat} (g/g)
p-xylene	1065	0.1303	1805.7	0.1094	1855.15	0.1032	1768.4	0.1104
m-xylene	229.9	0.1303	1310.2	0.0977	1234.58	0.0948	1251.7	0.0969
o-xylene	188.4	0.1303	1543.5	0.1046	1417.3	0.1012	1501.4	0.1008
ethyl benzene	306.7	0.1303	1297.7	0.0985	1335.9	0.0885	1234.6	0.1011
p-diethyl benzene	1293	0.1077	1781.9	0.0717	1528.9	0.0812	1768.42	0.0802

First Iteration (*k* = 1): Figure sets (d), (e) and (f) of Figure 9 show the concentration profiles in the first iteration and the corresponding ternary plots. In this iteration, the following

three tasks were carried out: 1. ten experiments that were determined in the initial iteration were carried out, 2. the model parameters were updated based on new experimental results, and 3. model simulation and optimization were repeated. The concentration profile underwent a significant change in this iteration. A wide range of compositions on the new concentration profile was exposed outside of the existing experimental measurements. From this updated concentration profile, compositions were selected to cover the new space. The values for the selected compositions are shown in Table 2 (experiments 11 to 16), and the corresponding experimental results are shown in the supporting information.

Comparing the empty diamonds and solid circles, one can notice that the newly selected compositions were in drastically different positions. In particular, the predicted concentration of *p*-xylene at approximately $x = 0.35$ was unusually high initially (Figure 9(a)), which is corrected in the first iteration (Figure 9(b)). This is because the competition between *p*-xylene and other components was overestimated in the original isotherm parameter, which was corrected by the experimental data of the breakthrough experiments at such compositions (Experiments #3, 4, and 5 in Table 2).

Second iteration ($k = 2$): Following the same steps as in the previous iteration, the selected compositions were tested in breakthrough experiments, parameters were updated, and the SMB process was simulated and optimized. Figure sets (g), (h) and (i) of Figure 9 show the result of the second iteration. In this iteration, the concentration profiles changed much less significantly. Only a small range of compositions in the new concentration profile was not covered by existing experimental measurements. The accuracy of the isotherm can be increased by increasing the density of experimental measurements. In this iteration, the composition selection should be tightened in order to obtain a more accurate measurement in this range. This is achieved by

decreasing the tolerance, δ_k, in the composition selection algorithm from 0.20 to 0.10. The combination of concentration profile changes and the decreasing of the tolerance value, δ_k, led the algorithm to select another six experiments to be conducted in the next iteration. The values for the selected compositions are shown in Table 2 (experiments 17 to 22) and, the corresponding experimental results are shown in the supporting information.

Third iteration (k = 3) and converged profile: When the compositions in the second iteration were tested by breakthrough experiments, the SMB model was optimized once more utilizing the new experimental results. As is shown in figure sets (j), (k) and (l) of Figure 9, the new composition profiles are similar to that in the previous iteration, and it can be described by all of the previously tested compositions. Since there is no significant change in concentration profile, it is determined to be the final and optimal profile. It should be noted that decreasing the value of δ_k may not lead to further improvement since the magnitude of measurement error may exceed the tolerance. If the iteration were to be continued, the concentration profile predicted by the process model may keep changing due to the uncertainty of experimental measurements (Figure S1). Therefore, further iterations would yield little improvement on the existing isotherm and model prediction.

In total, 22 experimental measurements were carried out to reach the final isotherm and optimal SMB operation. This can be a significant reduction in experimental effort compared to a traditional factorial design approach. If the greater accuracy of an isotherm is desired, the number of experiments in the factorial design approach increases exponentially while that in the proposed approach increases much slower.

3.3.2 Improvement of Isotherm Fitting

The adsorption data of the compositions were fitted to the extended-Langmuir isotherm by the least square method given in section 3.3.2. Figure 10 shows the least square fitting of the experimental data to Langmuir isotherm. During each iteration, liquid compositions that were on the SMB internal concentration profile ($\zeta_{k,p} = 1$) were fitted to the extended-Langmuir isotherm model. Other liquid compositions that were tested by breakthrough experiments but were off the current simulated SMB concentration profiles ($\zeta_{k,p} = 0$) did not participate in the isotherm parameter estimation; they were plotted as a comparison. Figure 10 (a) shows the least square fitting of the adsorption data in the first iteration. Since there is no previously tested liquid compositions, three more compositions (R1, R2, and R3) that were off the concentration profile were randomly chosen and tested.

The fitting obtained for compositions on the concentration profile is good which indicates a good local adsorption model for the composition range in the first iteration. It can also be observed that the compositions that were not used for isotherm fitting had relatively poor fit. This indicates that the local model only described a small range near the optimal concentration profiles, and the compositions outside the range cannot be described accurately by a local model. This also indicates that the extended-Langmuir model cannot be used as a global isotherm model to describe the adsorption of the entire domain of liquid composition. As shown in Table 2, the compositions that participated in the isotherm parameter estimation (i.e. $\zeta_{1,p} = 1$) were experiments 1 to 10. The compositions that were tested but not included in the isotherm parameter estimation (i.e. $\zeta_{1,p} = 0$) were experiments R1, R2, and R3. Figure 10 (b) and (c) shows the isotherm fitting in the second and third iterations.

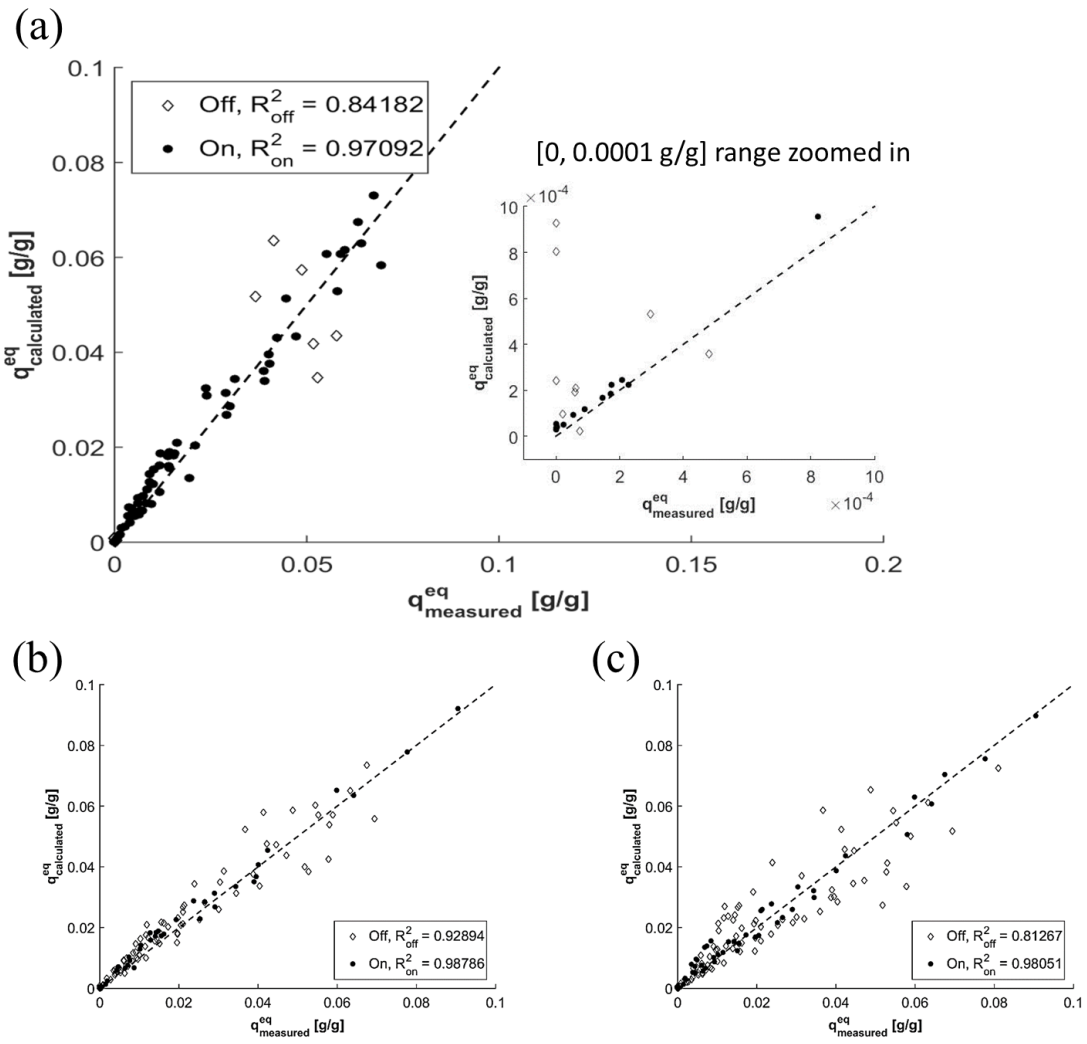

Figure 10 - Adsorbate concentration calculated from isotherm fitting vs. adsorbate concentration measured by breakthrough measurements for three iterations. (a) least square fitting for the first iteration; (b) least square fitting for the second iteration; (c) least square fitting for the third iteration; Solid circles: compositions that lie closely on the simulated concentration profile; Empty diamonds: compositions that are not on the simulated concentration profile

To quantify the fit, the R^2 values for compositions on the concentration profile were always found to be above 0.90 for "On" compositions. It should be noted that the R^2 values were not related to the convergence of the approach, and it does not necessarily increase as the iterations proceed. The R^2 value is calculated only to confirm the accuracy of the local model for the local region (denoted as "on" in Figure 10 in each iteration. For example, the R^2 value for compositions

on the concentration profile in the 2nd iteration was higher than that in the 3rd iteration. The higher value only means the local model was more accurate in that particular range, which is not necessarily close to that in the optimal SMB operation. In fact, the experimental accuracy was limited by the degradation of the sieve over time (figure S1); and within experimental error, the local models were similarly accurate.

The compositions that were on the concentration profile and participating the parameter fitting were labeled with $\zeta_{k,p} = 1$, for each iteration, k, and each experimental measurement, p. Table 2 summarize the values for $\zeta_{k,p}$, during each iteration. The corresponding adsorption data of each experiment are given in the supporting information.

3.3.3 Convergence of Optimal Operating Condition

Figure 11 shows the optimized SMB operating conditions for all iterations. The shaded region in this figure represents the set of conditions that achieve the required purity and recovery of 99.7% and 97.0%, respectively, using the parameters in the final iteration (k = 3). Furthermore, the optimal operating condition that achieves the highest throughput, without constraining the desorbent consumption, was plotted on the same figure. It can be observed that the initial SMB operation, which was optimized using the initial isotherm parameters, was far from the optimal solution obtained using the final isotherm parameters. In addition, the optimal SMB operation in the last two iterations is similar to each other, indicating the convergence of this iterative-concurrent approach.

3.4 **Design Variations and Parameter Uncertainty**

In this section, I consider design variations in the proposed method. Process design usually includes many variations to consider multiple scenarios depending on the product demand and prices. With the final isotherm data, a sensitivity analysis was done with respect to design variance. Case studies in different SMB process design scenarios, including different levels of purity, recovery, feed compositions, and desorbent to feed ratio (D/F ratio), were carried out. It should be noted that sensitivity analysis for purity and feed compositions of xylenes are particularly useful when hybrid separation processes that combine different separation techniques [59, 60] are considered.

In addition, model robustness against parameter uncertainty was taken into consideration. Sensitivity analysis was applied to the changes in feed compositions and mass transfer coefficient. Since normally there were more dead volumes in the SMB apparatus than in a single column liquid chromatography system, the apparent mass transfer may be different compared to the measured mass transfer coefficient from single column experiments. To consider such an influence, the impact of mass transfer coefficients on model prediction was studied. In addition, feed to the SMB may be from different sources and may vary during operation. The sensitivity of the model to feed compositions was also studied.

Table 2 - Summary of values for the binary variable, $\zeta_{k,p}$, during each iteration for each measurement.

Experiments #	1st iteration $\zeta_{1,p}$	2nd iteration $\zeta_{2,p}$	3rd iteration $\zeta_{3,p}$	*p*-xylene (%)	*m*-xylene (%)	*o*-xylene (%)	ethyl benzene (%)	*p*-diethyl benzene (%)
1	1	1	1	22.1	0.3	0.2	0.1	75.1
2	1	0	0	38.8	0.3	0.2	0.1	58.4
3	1	0	0	48.5	0.1	0.0	0.0	49.2
4	1	0	0	58.4	10.0	5.3	5.2	19.6
5	1	1	1	0.1	29.7	14.6	14.6	38.4
6	1	1	1	0.0	19.8	9.7	9.8	58.3
7	1	0	0	51.0	12.0	0.9	22.6	12.4
8	1	0	0	28.2	26.9	2.7	33.4	7.8
9	1	0	0	20.6	45.5	9.7	19.3	3.9
10	1	0	0	3.7	49.2	13.0	15.1	18.0
11	-	1	0	17.9	33.8	8.1	16.6	22.0
12	-	1	1	0.0	9.8	4.8	4.8	78.2
13	-	1	1	0.1	0.6	0.2	0.1	96.4
14	-	1	1	26.6	8.1	6.8	2.2	54.0
15	-	1	1	24.8	17.8	9.0	4.9	41.4
16	-	1	1	17.6	5.1	5.0	1.0	68.8
17	-	-	1	11.7	0.0	0.0	0.0	86.0
18	-	-	1	5.0	41.0	14.3	12.1	24.9
19	-	-	1	17.7	24.8	17.8	6.2	31.3
20	-	-	1	13.5	32.5	11.8	8.8	31.2
21	-	-	1	1.0	34.0	10.4	8.6	43.7
22	-	-	1	0.0	19.9	4.8	5.8	67.3
Ref. 1 (R1)	0	0	0	0.6	0.9	0.2	46.6	48.8
Ref. 2 (R2)	0	0	0	0.1	0.2	51.2	0.4	45.3
Ref. 3 (R3)	0	0	0	0.0	45.1	0.4	50.6	0.2

Here, I use process model optimization as the means to study the sensitivity of the process mode. For each case, I constrain the model with different design specifications or use different model parameters. Then the process is optimized without changing SMB performance indicators (purity, recovery, etc.) because I wished to investigate the change of optimal concentration profile. The change of optimal concentration profile may lead to different experimental

measurements that need to be carried out, and it is desirable to know if the model is robust enough that can be used in multiple scenarios without increased experimental efforts.

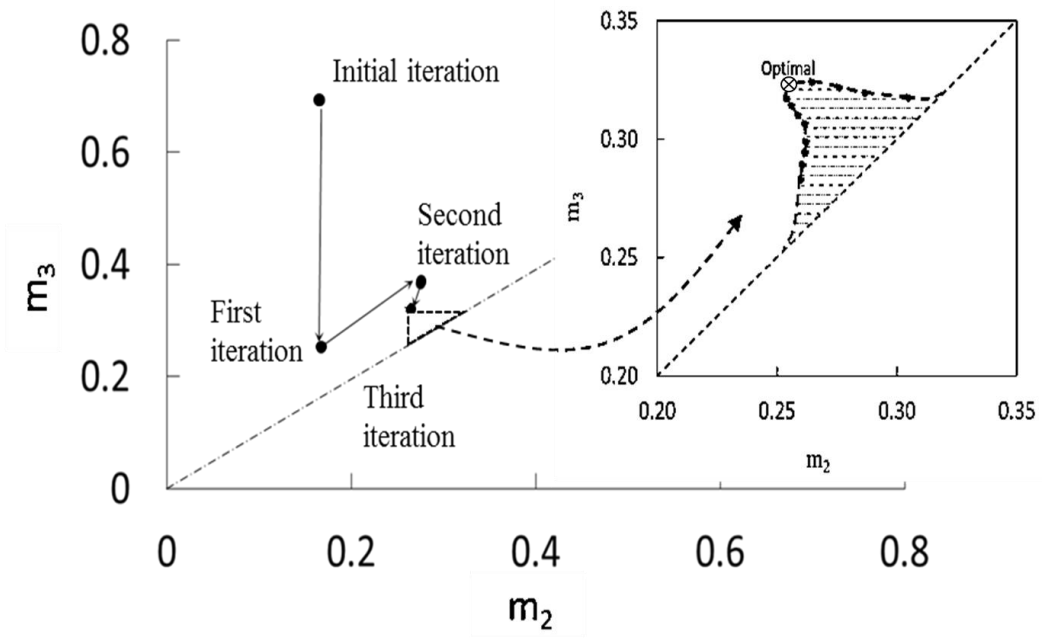

Figure 11 - Trajectory of Operating Conditions

3.4.1 Model Sensitivity to design variations in Purity, Recovery and D/F ratio

The internal concentration profiles of the optimized SMB for the purities of 90.0%, 95.0%, 99.6%, 99.7%, and 99.8% were obtained using the final isotherm parameters (Figure 12 (a)). For xylene separation by SMB for purities of 99.6%, 99.7%, and 99.8%, the change of the concentration profiles is relatively minor indicating the obtained parameters can be used for the design of purities in this range. However, for even lower purity (90.0% and 95.0%), the loop of concentration profiles becomes larger and outside the range of compositions tested in the breakthrough experiments. Nevertheless, in this study, the entire trajectory of the new concentration profile can be mostly covered by adsorption data in the previous iterations (k = 0, 1, and 2) for the final value of the tolerance parameter, δ = 0.10. Therefore, the adsorption

information for these concentration profiles can be easily obtained by merely refitting the isotherm parameters after carrying out only a few additional breakthrough experiments. It should finally be noted that such an observation may not be generalized, and additional breakthrough experiments may be necessary if the concentration profiles in the SMB are more sensitive to purity, recovery, and D/F.

Figure 12 (b) shows the internal concentration profiles of the optimized SMB designed with recoveries of 80%, 90%, 95%, 96%, 97%, and 98% based on the final isotherm parameters. It can be observed that the SMB design was robust against changing recovery. In all these cases, $\overrightarrow{C_k}(x)$ on the new concentration profiles were covered by previous experimental measurement completely for the final value of the tolerance parameter, $\delta = 0.10$. Thus, it was not necessary to re-characterize isotherm parameters for the new compositions.

Figure 12 (c) shows the simulation of SMB design with D/F of 2.0, 3.0 and 4.5. With a smaller value of the D/F ratio, the concentration profile loops expand, but similar to other cases, almost the entire trajectory of the new concentration profile was covered by existing adsorption data for the final value of the tolerance parameter, δ = 0.10. A few additional experiments may need to be carried out to maintain the same accuracy. If the operation at a different value of D/F is employed, the local isotherm model may need to be updated by reassigning different values of $\zeta_{k,p}$ and carrying out the regression.

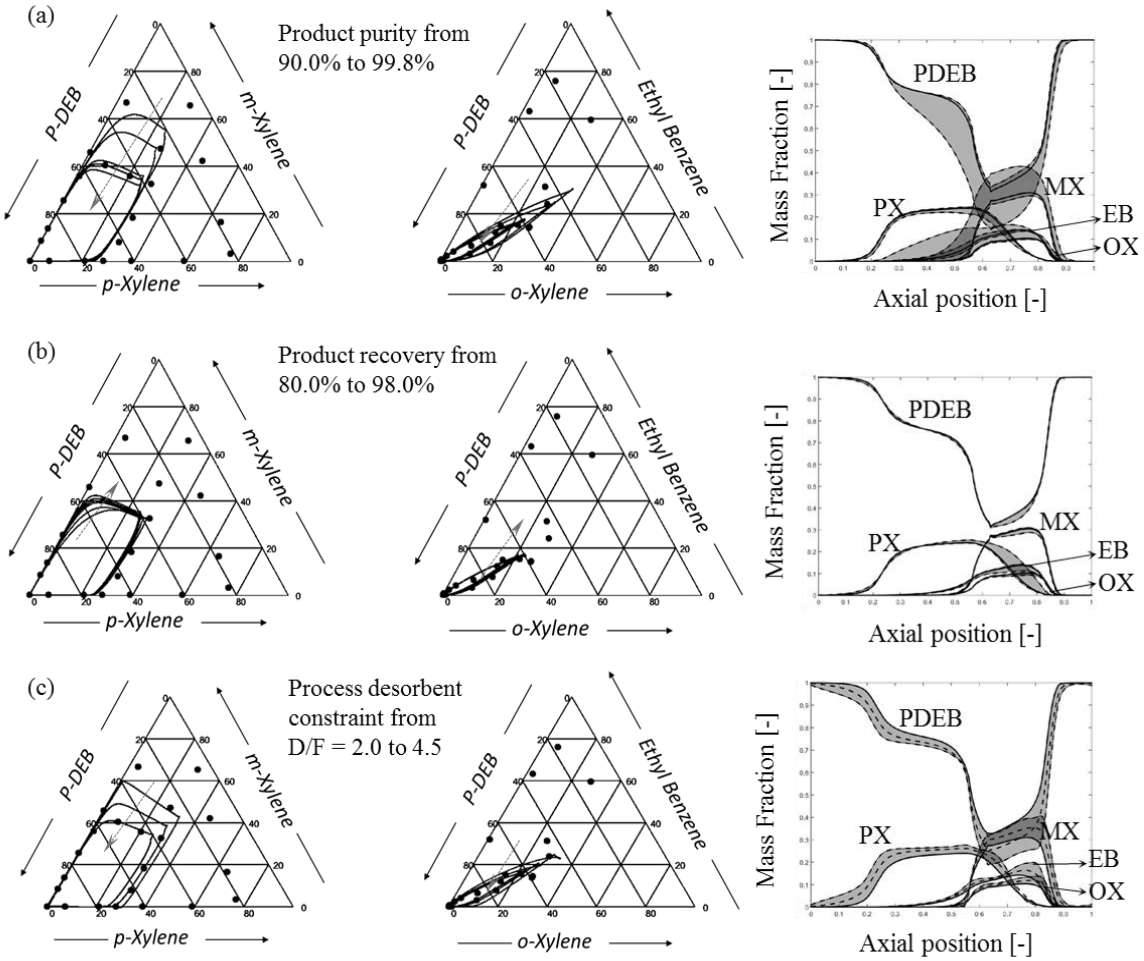

Figure 12 - Ternary plot of simulated concentration profiles. (a) sensitivity analysis with respect to changes in product purity; (b) sensitivity analysis with respect to change in product recovery; (c) sensitivity analysis with respect to changes in process desorbent consumption requirement.
Solid circles: chemical compositions that were tested by adsorption experiments;
Solid curves: SMB internal concentration profiles at different scenarios;
Dashed arrows: the direction of concentration profile change with respect to the increase of design parameters.
Solid curves on SMB internal concentration plot: concentration profile of the base case;
Dashed curves: concentration profile of the other cases; shaded areas: area of possible concentration profile change within the range of the present sensitivity study.

3.4.2 Model sensitivity to parameter uncertainty (mass transfer coefficient and feed inlet compositions)

Depending on the particle size and binder materials used for the BaX zeolite, the mass transfer can be significantly different. The SMB process also has dead volumes whose effect can

be lumped into the mass transfer coefficient [15]. Usually, mass transfer coefficients can be the most unpredictable and uncertain parameter for SMB design.

Figure 13 (a) shows the internal concentration profiles of the optimized SMB process with mass transfer coefficient of 1 min^{-1}, 2 min^{-1}, 3 min^{-1}, 4 min^{-1}, 5 min^{-1}, and 6 min^{-1}. Surprisingly, all the concentration profiles overlap as long as flow rates and switching time are allowed to adjust to compensate for different mass transfer coefficients, which indicates that there exists only a single set of optimal concentration profiles for all mass transfer coefficient in the range studied. In these cases, while the operating conditions and internal concentration profiles of the optimal SMB design change significantly for different values of mass transfer coefficients, the range of compositions, shown as trajectories in the triangle diagrams, are not sensitive to mass transfer coefficients. This fact indicates that additional experiments are not necessary even if a wide range of mass transfer coefficients is considered.

In order to study the sensitivity of the approach, a few arbitrary feed compositions (Table 3) were simulated (Figure 13 (b)). Mixed xylenes can be obtained from different sources, such as catalytic reformate, pyrolysis gasoline, toluene disproportionation product, and coke-oven light oil[61]. Some sources of mixed xylenes have a high concentration of EB; some contain less. It was observed that the SMB concentration profile was highly sensitive to feed composition. This fact indicates that for accurate isotherm modeling, either the range of feed compositions should be narrowed down at a relatively early stage of process development, or the breakthrough experiments must be performed covering a wide range of different compositions.

Table 3 - Three feed compositions (chosen arbitrarily)

	p-xylene	*m*-xylene	*o*-xylene	Ethyl benzene
Base case (1)	23.6%	49.7%	12.7%	14.0%
Case (2)	15.0%	50.0%	10.0%	25.0%
Case (3)	27.0%	57.0%	14.0%	2.0%

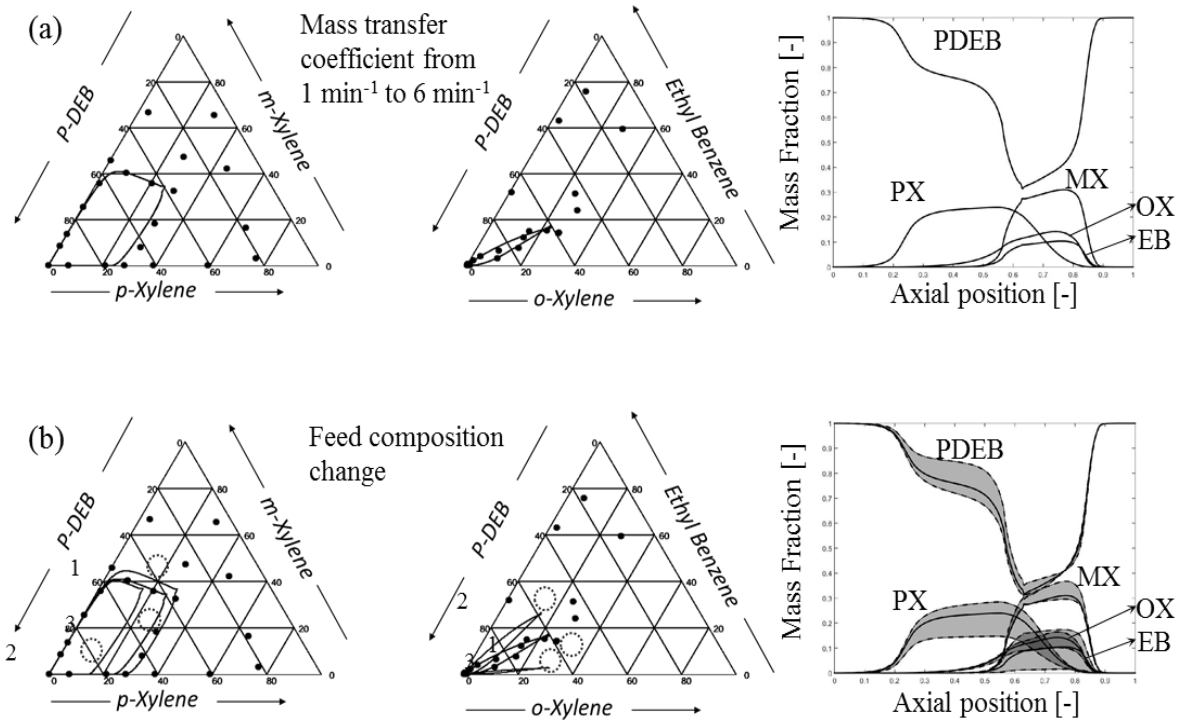

Figure 13 - Ternary plot of simulated concentration profiles. Solid circles: chemical compositions that were tested by adsorption experiments; Solid curves: SMB internal concentration profiles at different scenarios; Different cases were numbered. Solid curves on SMB internal concentration plot: concentration profile of the base case; dashed curves: concentration profile of the other cases; shaded areas: area of possible concentration profile change within the range of sensitivity study.

3.5 Conclusion

An iterative-concurrent approach was developed to improve the robustness of SMB process model prediction. After iterations of the experimental validation and model prediction, the isotherm determination and predicted SMB operation converge. In this approach, I was able to obtain the optimal SMB operating conditions and the corresponding internal concentration profiles. Breakthrough experiments were performed based on the model prediction for each iteration, and 22 measurements were used to model a multicomponent isotherm, which can be a significant reduction of experimental effort. The parameter fitting by the least square method was applied for each iteration to update the isotherm. While the simple Langmuir isotherm was sufficient as a local model, the local model may need to be updated when the range of compositions are significantly different. With the more accurate isotherm for the expected internal compositions in the process, it is expected that the SMB process model is more accurate than the one developed in a conventional method where isotherm measurements were carried out at compositions determined heuristically. With such a more accurate model, pilot plant validation would also be more efficient.

Future work would involve comparing the model prediction by this approach with experimental results from a lab-scale SMB apparatus. In the next Chapter, I perform this important step with a different system: aromatics separation from alkanes. The iterative-concurrent approach can be readily applied to other multicomponent adsorption systems and other separation processes, such as TSA or PSA. Moreover, this approach can be expanded to include temperature gradient, pressure gradient, salt/pH gradient in separation processes [62, 63]. These extra variables can be handled within the proposed framework by treating them as extra dimensions of the experimental design. Therefore, the proposed approach can reduce the number

of experimental conditions that need to be tested. I would also like to adapt this rapid process design approach to be used in material screening. When comparing the process efficiency based on several newly developed/discovered adsorbent materials, an approach that requires a minimal amount of material and experimental effort is critical. This approach has the potential to provide a rigorous performance comparison of materials in the actual chemical process. In Chapter 5, I also investigate the expansion of the present approach to more complex systems that involve greater than five components.

CHAPTER 4. AROMATICS/ALKANES SEPARATION: SIMULATED MOVING BED PROCESS MODEL DEVELOPMENT BY A CONCURRENT APPROACH AND ITS VALIDATION IN A MINI-PLANT

4.1 Motivation

I initially developed the concurrent approach for the separation of xylene isomers [64]. In this work, I would like to generalize the method to the separation of components that are significantly different in terms of physical properties and adsorption behaviors. In particular, reformate streams containing a mixture of aromatics and alkanes (linear and cyclic) which may have a substantial number (>30) of components with overlapping boiling points [11]. The separation of reformed aromatics from alkanes is an interesting and useful target for SMB processes. Towards this end, in this work, I have used a ternary aromatic-linear alkane-cycloalkane mixture as a model system. Specifically, I study the separation of toluene and dodecane using cyclohexane as desorbent, with an aromatic-selective silica gel (Davisil Grade 923) adsorbent. In this model system, strong competition exists among all three components, which requires careful development of the concurrent approach and adsorption model isotherm. This work has two main features: first, I implement the concurrent approach in this system and obtain an SMB process model with minimal experimental effort; and second, I validate this approach experimentally for the first time using a 16-column SMB “mini-plant”.

4.2 Concurrent Approach with SMB mini-plant testing

The concurrent approach was modified in this work to include SMB prediction and plant-specific parameter determination. Figure 14 illustrates the workflow of applying the concurrent approach for SMB separation of toluene and dodecane. The details of each step are explained in the next section. The approach consists of two stages; in the first stage, I develop the isotherm model, and in the second stage, I estimate kinetic and plant-specific parameters from the SMB mini plant. The first stage of the proposed approach includes steps from *Step 1* to *Step 5*, and the methodology in this stage is similar to the previous work.

The second part of the proposed approach starts after *Step 5* converges. In *Step 6*, the obtained SMB operating conditions are validated experimentally on the SMB mini-plant. In this experiment, the outlet concentrations (extract, raffinate and recycle), as well as the internal liquid flows, are sampled and analyzed to obtain the concentration profiles of all components in the system. In *Step 7*, the measured concentration profiles are compared against the model prediction. If the model is sufficiently accurate, the process development is terminated at this step. On the other hand, if a large discrepancy is detected, the kinetic and plant-specific parameters (mass transfer coefficients and dead volumes) are updated. In Step 8 a new operating condition is predicted again using the updated parameters, and the procedure is repeated from *Step 6*.

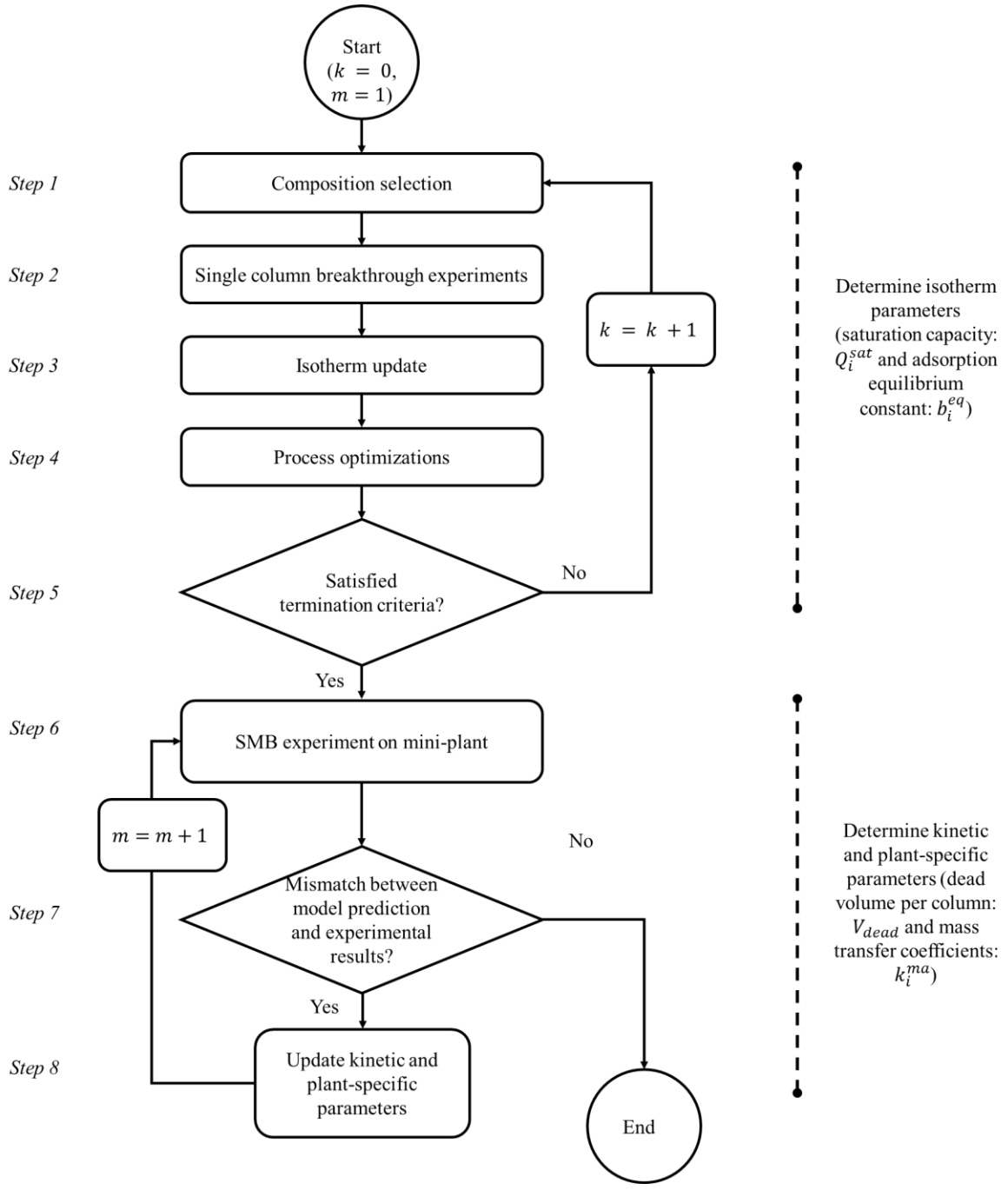

Figure 14 - Illustration of the iterative approach of concurrently finding SMB optimal operating conditions while developing the adsorption isotherm. k is the index for iterations during isotherm determination process. m is the index for iteration during kinetic and plant parameter determination process.

4.3 **Methodology**

Most of the methods (experimental and modeling) used in this chapter were similar to those in Chapter 3. There are some modifications to the previous study, and the differences are discussed here.

4.3.1 Composition Selection Algorithm Modifications

In addition to the isotherm parameters, plant-specific parameters which cannot be estimated from the breakthrough experiments must also be considered as additional cases. In this study, I consider the influence of the mass transfer coefficients and the dead volume. It was assumed that the range of the dead volume V_{dead} was between 0-2.5% of column volume V_c, and the range of the mass transfer coefficients k^{ma} was between 0.5-2 min^{-1}. By selecting a few values in these ranges and creating a list of combinations, a total of 54 cases ($case^{MAX}$ = 54 in Figure 15) were considered in the composition selection algorithm. The algorithm was first applied to the base case (*case* = 1) wherein k^{ma} of all components were set to 1 min^{-1}, and dead volume was set to 0%. Then the composition selection algorithm was applied to all other cases (*case* = 2, 3, …, 54) with the mass transfer coefficients listed in Table 4.

Table 4 - Values of mass transfer and dead volume parameters used composition selection.

Dead volume [%]	$\boldsymbol{k^{ma}_{toluene}}$ **[min^{-1}]**	$\boldsymbol{k^{ma}_{dodecane}}$ **[min^{-1}]**	$\boldsymbol{k^{ma}_{cyclohexane}}$ **[min^{-1}]**
0.0 and 2.5	0.5, 1.0 and 2.0	0.5, 1.0 and 2.0	0.5, 1.0 and 2.0

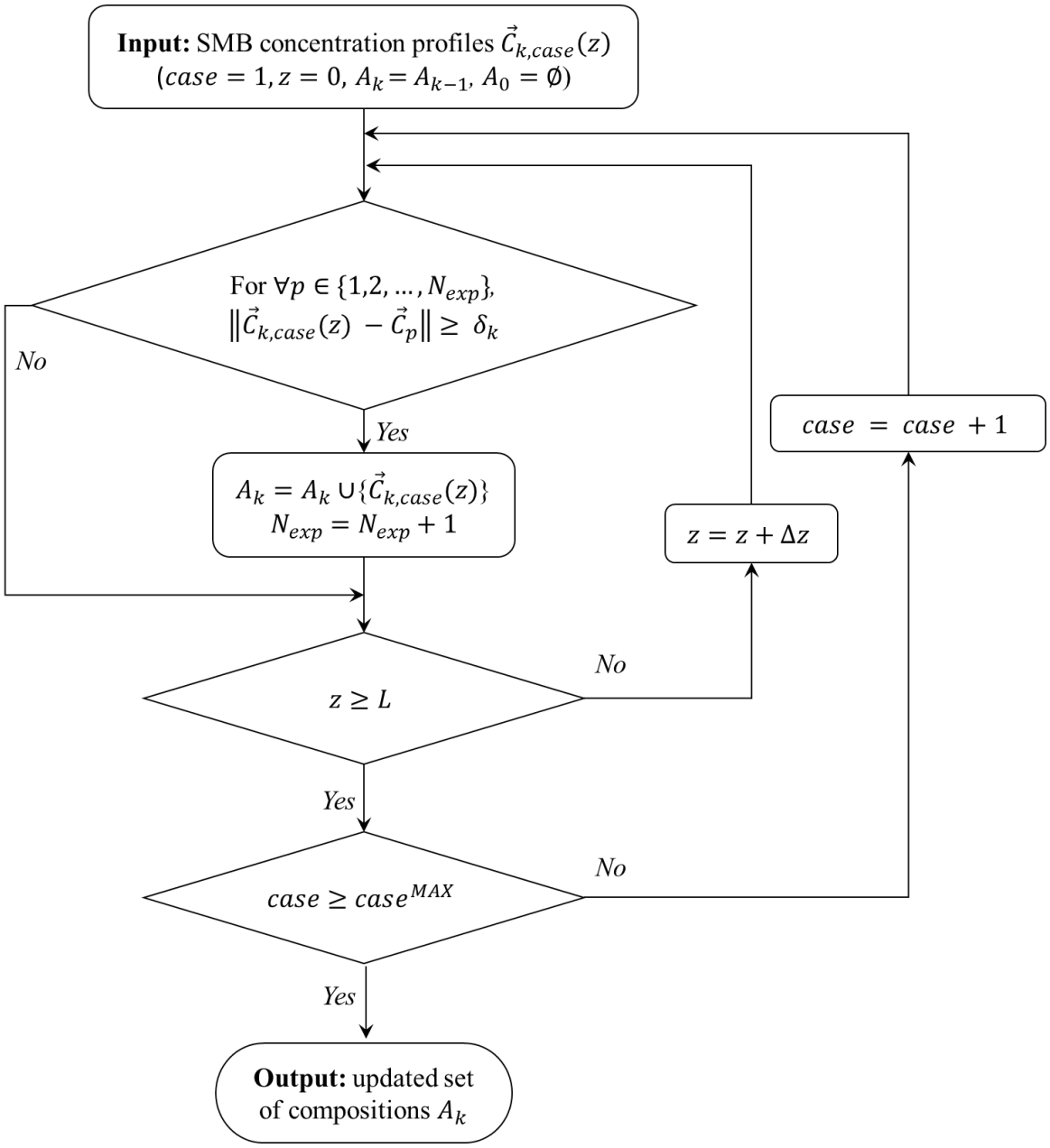

Figure 15 - Composition selection algorithm for breakthrough experiments.

4.3.2 Breakthrough Experiments

The analysis of breakthrough results was changed due to the lack a reliable tracer. Figure 16 shows a typical multicomponent breakthrough curve. Since I were not able to find a useful tracer molecule for this system, the dead volume was determined prior to the experiments based

on the known adsorbent density and pore volumes estimated by the bed volume and measured bed weight. The bed void ratio calculated in this manner was 0.387.

The density of the adsorbent was calculated as follows:

$$\rho_{adsorbent} = \frac{m_{adsorbent}}{V_{pore} + V_{skeleton}} = \frac{m_{adsorbent}}{m_{adsorbent}\delta_{pore} + \frac{m_{adsorbent}}{\rho_{skeleton}}} \quad (24)$$

where $m_{adsorbent}$ is the mass of the adsorbent packed into the column (unit: g), V_{pore} is the volume of the pores of the adsorbent (unit: cm^3), $V_{skeleton}$ is the volume of the solid of the adsorbent (unit: cm^3), $m_{adsorbent}$ is the mass of adsorbent (unit: g), δ_{pore} is the pore volume per mass of the adsorbent provided by the vendor (unit: cm^3/g), and $\rho_{skeleton}$ is the density of the solid skeleton of the adsorbent material which is measured using pycnometer (unit: cm^3/g). After the density of the adsorbent was calculated, the void fraction of the column can be calculated as follows:

$$\varepsilon_{void} = \frac{V_{bed} - V_{adsorbent}}{V_{bed}} = \frac{V_{bed} - \frac{m_{adsorbent}}{\rho_{adsorbent}}}{V_{bed}} \quad (25)$$

where V_{bed} is the inner volume of the column, and $V_{adsorbent}$ is the total volume of the adsorbent (including the pore volume and the solid skeleton volume). The total time for a non-retained component to go out of the column consists of the time that the component stayed in the system volume, V_{system} (i.e. tubing, after the injection valve and before the detector) and the time that the component spend in the void fraction of the column, V_{void}.

$$V_{delay} = V_{system} + V_{void} = V_{system} + \varepsilon_{void} V_{bed} \quad (26)$$

Table 5 shows the properties of the adsorbent that were used to calculate the total delay volume. The mass of the adsorbent packed in the columns was measured after activation and before the breakthrough experiments. The density of the adsorbent skeleton was measured using pycnometer. The adsorbent pore volume was obtained from the vendor specifications.

Table 5 - Properties of the adsorbent.

Mass of adsorbent	$m_{adsorbent}$	9.80 g
Density of the adsorbent skeleton	$\rho_{skeleton}$	2.137 $\frac{g}{cm^3}$
Adsorbent pore volume	δ_{pore}	0.40 $\frac{cm^3}{g}$
Total bed volume	V_{bed}	13.88 cm^3
System volume	V_{system}	2.60 cm^3

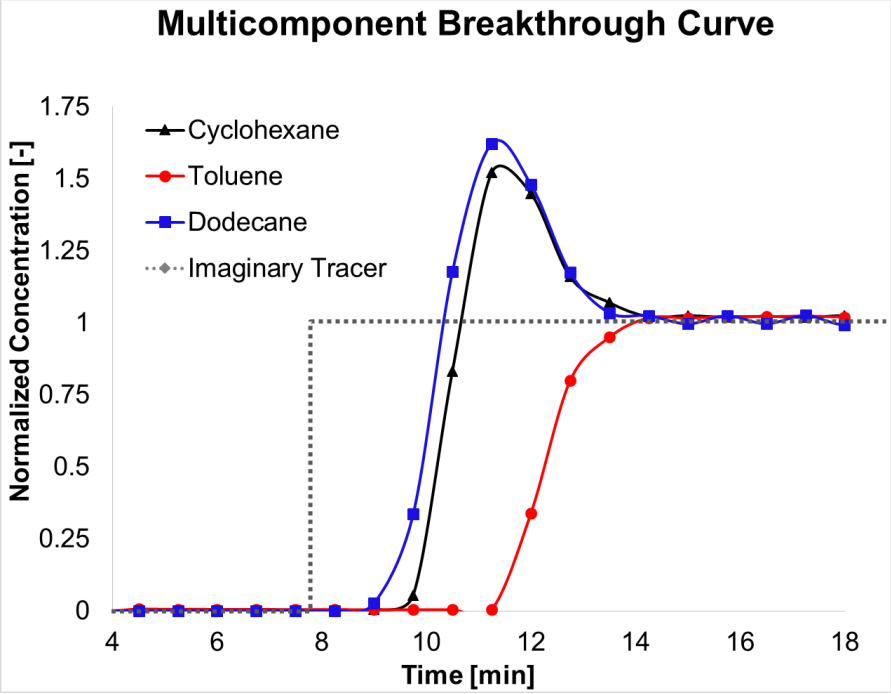

Figure 16 - A typical breakthrough curve of the toluene-dodecane-cyclohexane mixture on silica gel adsorbent at 30 ºC and 100 psig. The column was initially filled with n-heptane

Furthermore, I measured the system dead volume by UV-Vis spectroscopy after replacing the column by a zero-dead-volume union and obtained a value of 2.33 cm^3. This dead volume is a significant fraction of the column volume (13.88 cm^3) and cannot be ignored. Equation 27 was used to obtain the amounts adsorbed at equilibrium from the breakthrough curves. The dashed line in Figure 16 is the breakthrough curve of an imaginary tracer, which is assumed to have zero capacity and infinitely fast mass transfer rate based on the calculation of the total delay volume V_{dead}. Using this volume, I estimate the equilibrium adsorbed concentration q_i^{eq} as follows:

$$q_i^{eq} = C_i^{in}(F\Delta t - V_{dead}) - F\int C_i^{out}dt \tag{27}$$

Here, F^{in} and F^{out} are inlet and outlet flow rates and they were assumed to be the same, which was confirmed experimentally using a mass flow controller ($F^{in} = F^{out} = F$); C_i^{in} and C_i^{out} are

the inlet and outlet concentrations of components; V_{dead} is the total dead volume (system dead volume plus bed void fraction volume).

4.3.3 SMB Experiments (Step 6)

In this study, I included SMB experiments as a validation step. The design of the SMB mini-plant constructed in our laboratory is shown in Figure 17. Columns were assembled in the same manner as that in the breakthrough experimental set-up. Valves (switching valve: EUDB-C6UW, dead-end selector: EUTB-6CSD16MWE, flow-through valve: EUTB-6CSF16MWE, and flow-trapping valve: EUTB-6CST16MWE) were purchased from Valco Instruments Co. Inc. (Houston, TX, USA), and were all electronically actuated. Cross manifolds (Z4M1), fittings and tubing were also purchased from Valco. The plant consists of 16 columns that are all connected to a flow-through valve. There were also five dead-end selector values used to control the inlet and outlet positions of feed, raffinate, extract, desorbent, and recycle. In addition, two pumps are used to deliver feed stream and desorbent stream. There are three mass flow controllers to control and measure the outlet flow rates of extract, raffinate, and recycle. The sampling of the internal liquid concentrations can be performed in this unit. All 16 columns are connected to an A/B switching valve which is connected to a flow-trapping valve. During normal operation, the flow goes through the SS valve and by-pass the ST valve. The SS valve is switched when sampling is carried out so that the liquid flow goes through the sample loops attached to the ST valve. When switching of the inlet and outlet ports (feed, desorbent, extract, raffinate, and recycle) occurs, the ST valve switches together, thus trapping the internal liquid. In this work, I carried out the sampling for an entire cycle that consists of 16 steps, resulting in 16 different liquid compositions. These samples represent the internal concentration profile of the SMB for all 16 steps at a fixed location. All parts are controlled by MATLAB scripts developed in-house.

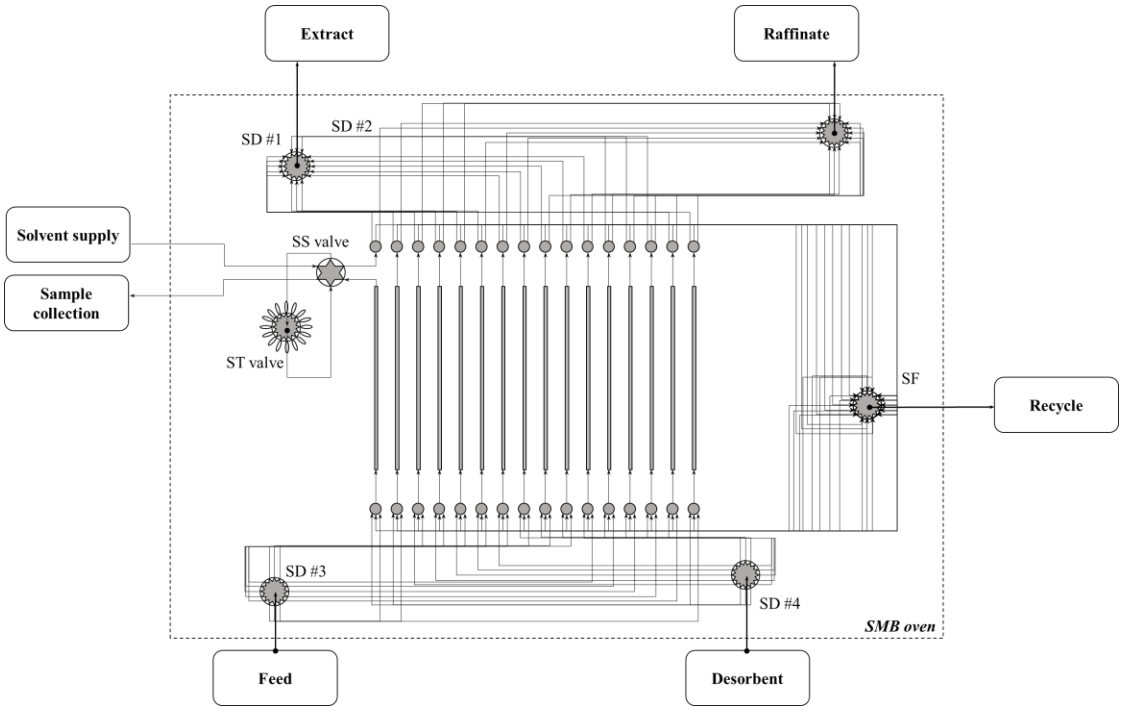

Figure 17 - SMB mini-plant schematic. SF: flow through valve (Valco); SD: dead end selector (Valco); ST: flow trapping valve (Valco); SS: 6-port switching valve (Valco).

4.3.4 Convergence Criteria for the Determination Optimal Operating Condition (Step 7)

Until the desired purity and recovery specifications are obtained, additional SMB experimental iterations are performed to estimate the kinetic and plant-specific parameters more accurately. SMB internal concentration profiles were also measured to further analyze the quality of the match between predictions and experiments and to obtain data for parameter fitting.

4.3.5 Estimation of Kinetic and Plant-specific Parameters by Least Squares Method (Step 8)

In this step, I estimate the mass transfer coefficients and dead volume in the SMB unit by comparing the internal concentration profile sampled in SMB mini-plant experiments against that from the process model. In this work, the following objective function was considered:

$$\text{minimize}_{\theta} \sum_{\substack{i=1 \\ n=1}}^{\substack{N_{comp} \\ N_{measure}}} \left(\left(C_{i,n}^{exp} - C_{i,n}^{model} \right)^2 \right) + M' \cdot \sum\nolimits_j \left(\frac{\theta_j - \theta_j^0}{\theta_j^0} \right)^2 \qquad (28)$$

where the parameter vector (variable) is given by $\theta_j = (k_{toluene}, k_{dodecane}, k_{cyclohexane}, V_{dead})$. As in the estimation of isotherm parameters, a regularization term was also introduced here. Once again, the regularization parameter M' was chosen by a few trial and error attempts such that the objective function was minimized while maintaining all decision variables in a physically reasonable range.

4.4 **Results and Discussion**

The results of each iteration are overviewed in Figure 18 (concentration profiles) and Figure 19 (isotherm refinement). The concentration profiles in Figure 18 are plotted in ternary composition diagrams as well as in the form of SMB column profiles. On the ternary composition diagrams, selected compositions for breakthrough experiments (generated in *Step 1*) are indicated. Figure 19 shows the isotherm parameter fitting for the equilibrium capacities of all the compositions measured experimentally at each iteration in *Step 2*. The experimentally obtained capacities were fitted to a multicomponent competitive Langmuir isotherm (*Step 3*), and Table 6 shows the isotherm parameters refined in each iteration. Figure 20 shows the operating conditions plotted on the "m_2-m_3" plane (also generated in *Step 4*).

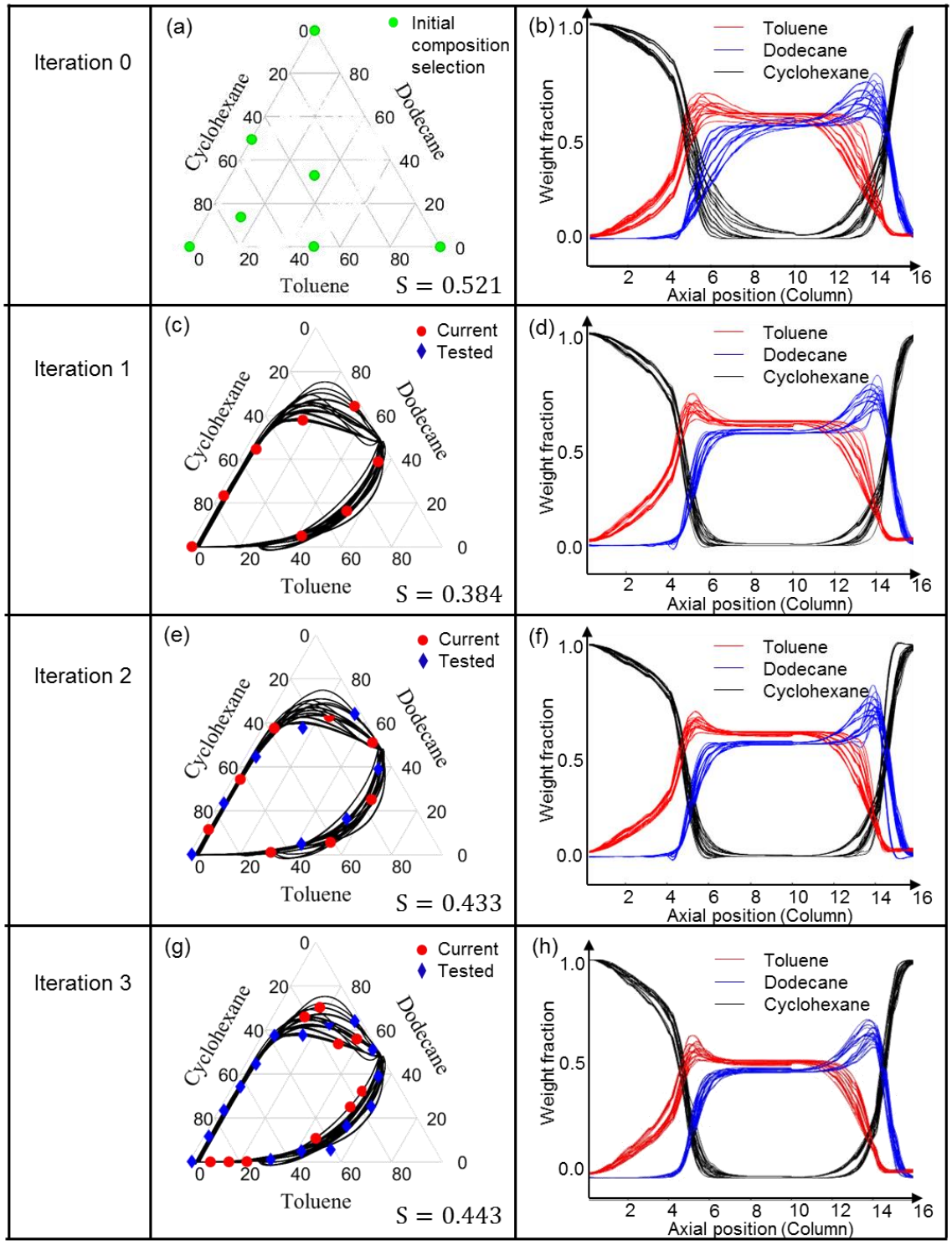

Figure 18 - Concentration profiles and selected compositions.

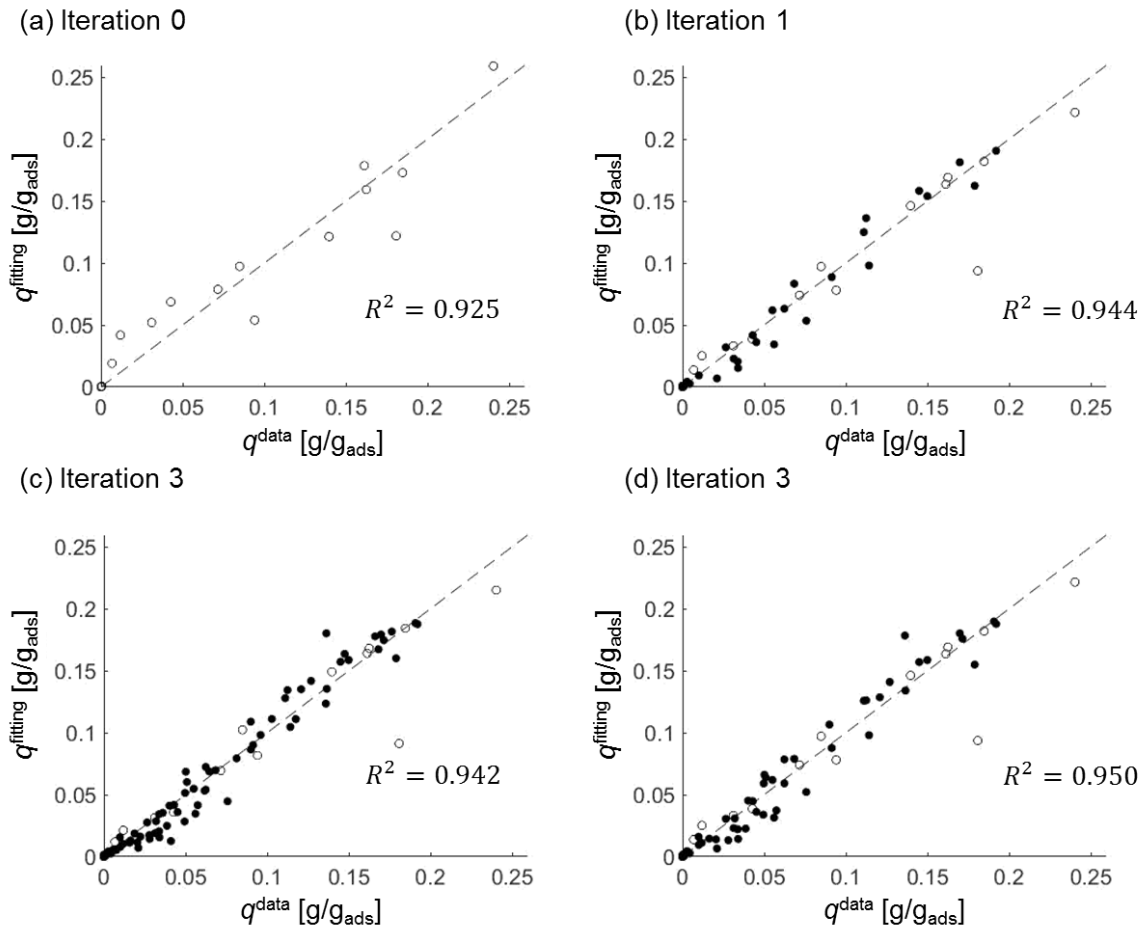

Figure 19 - Iterative isotherm refinement. R^2 represents the coefficient of the determination; empty circles represent compositions tested but not used in the final isotherm (compositions selected for initial iteration); solid circles represent compositions tested and used in the final isotherm.

Table 6 - Isotherm parameters refined at each iteration.

		Cyclohexane	Dodecane	Toluene
Iteration 0	b^{eq} [cm^3/g]	1061	866	1494
	Q^{sat} [g/g$_{ads}$]	0.206	0.200	0.299
Iteration 1	b^{eq} [cm^3/g]	845	479	2555
	Q^{sat} [g/g$_{ads}$]	0.184	0.255	0.252
Iteration 2	b^{eq} [cm^3/g]	887	591	2523
	Q^{sat} [g/g$_{ads}$]	0.189	0.212	0.255
Iteration 3	b^{eq} [cm^3/g]	813	476	2564
	Q^{sat} [g/g$_{ads}$]	0.189	0.215	0.248

4.4.1 Iteration 0 (k = 0)

With no prior knowledge of the adsorption behavior of the components on silica gel nor the SMB internal concentration profile, I started with measuring isotherms at a few compositions selected heuristically (Figure 18a). I selected pure toluene, dodecane, and cyclohexane, as well as four additional mixtures. Here, let's introduce the quantity *S* which represents how "spread-out" the tested liquid compositions are. The definition of *S* is given below:

$$S =< \left\| \vec{C}_p - \vec{\mu} \right\| >= \frac{1}{N_{EXP}} \sum_{p}^{N_{EXP}} \left\| \vec{C}_p - \vec{\mu} \right\| \tag{29}$$

$$\vec{\mu} =< \vec{C}_p >= \frac{1}{N_{EXP}} \sum_{p}^{N_{EXP}} \vec{C}_p \tag{30}$$

where μ is the average of tested compositions, which represents the center of all the compositions, and *S* can be calculated by taking the average of all the distances from the tested compositions to the center. Here, *S* resembles the well-known mathematical definition of "variance" in one-dimensional form.

After selecting the compositions in Step 1, I proceed to Steps 2-5. At the seven compositions selected in Step 1, breakthrough experiments were conducted (Step 2). Measurements from the breakthrough tests for these 7 compositions lead to an estimation of the isotherm (initial isotherm, Step 3). The parameter fitting for the initial isotherm is shown in Figure 19a and the isotherm parameters in Table 6. The isotherm obtained from initial iteration was used to predict the SMB concentration profiles (Step 4) shown in Table 6. Since this is the first iteration, I then increase the iteration counter *k* by 1 and return to Step 1. Compositions tested in

this iteration were discarded since these compositions were randomly chosen and may not be located on the concentration profiles.

4.4.2 Iteration 1 (k = 1)

With the experimental data, I repeat Steps 1-5. For Step 1, I can now utilize the predicted SMB internal concentration profile obtained in the previous iteration in the composition selection algorithm. The tolerance value, δ_1, was set to be 0.25 in this iteration (*k = 1*). With this tolerance value, a total of 8 compositions were selected (Figure 18c). At these newly selected compositions, breakthrough experiments were again carried out and Figure 19b shows the parameter fitting using the additional breakthrough data. It can be observed that the fitting was improved over the initial iteration, as confirmed by the R^2 value. It is interesting to compare the quality of fitting with the "spread" of the tested liquid compositions. The selected 8 compositions in this iteration had a smaller *S* value compared to the initial iteration (S_1 = 0.384 in *k* = 1 vs. S_0 = 0.521 in *k* = 0). Again, this observation implies that the multicomponent Langmuir isotherm with constant parameters works well if applied in a limited range of liquid compositions. Some minor differences in the predicted concentration profiles can be observed by comparing Figure 18b and Figure 18d. On the other hand, the predicted operating condition (Figure 20a) changed much more significantly. Thus, in Step 5, I decide to perform another iteration.

4.4.3 Iterations 2 and 3 (k = 2, 3)

The second iteration (*k* = 2) proceeded as follows. In *Step* 1, the tolerance value in this iteration (δ_2) was set to be a smaller value of 0.15 to maintain the number of compositions to be measured in breakthrough experiments, thus improving the accuracy of the adsorption model. In this manner, another 8 compositions were selected and tested experimentally in *Step* 3. The R^2

value (Figure 19c) did not change significantly, which can be explained by the fact that the liquid compositions were more "spread out" (S = 0.433 in k = 2 compared with S = 0.384 in k = 1). The isotherm parameters updated in *Step* 3 are shown in Table 6. Using the updated parameters, I obtain updated SMB concentration profiles and optimal operating conditions (*Step* 5). It can be observed in Table 6 that the isotherm parameters only changed slightly between iterations 1 and 2, and furthermore the concentration profiles (Figure 18 f) and operating conditions (Figure 20a) show much less change.

The third iteration (k = 3) is briefly described as follows. Using a lower tolerance value δ_3 = 0.1, I identified 10 additional compositions (*Step* 1). After carrying out *Steps* 2-4, I find that the isotherm parameters (Table 6), concentration profiles (Figure 18h), and fitting quality (Figure 19d) remain nearly unchanged from the previous iteration. The operating conditions were almost unchanged from the previous iteration. These observations led to our decision in Step 5 that the convergence is reached, and I proceed to the SMB mini-plant operation in Step 6.

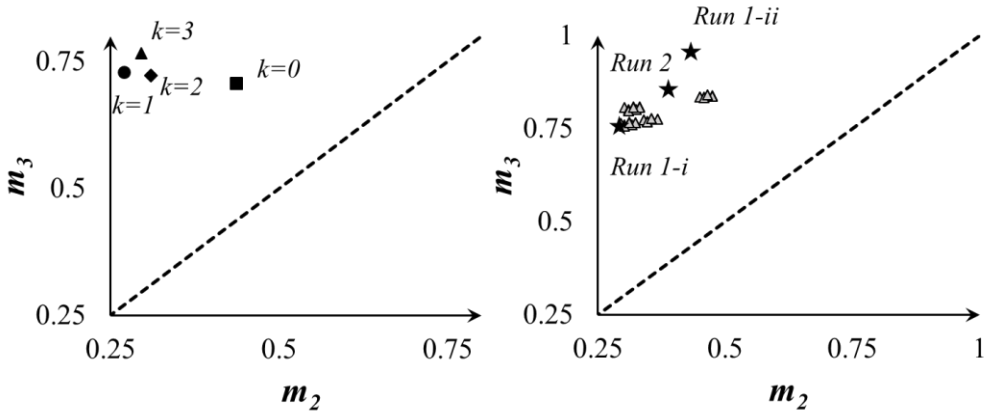

Figure 20 - SMB operating conditions plotted as dimensionless flowrates. (a) optimal operating conditions obtained using updated isotherm parameters for case = 1; (b) operating conditions implemented experimentally (stars), and optimal operating conditions for varied mass transfer and dead volume parameters.

4.4.4 SMB Experiments (Step 6-8)

After the isotherm parameters are determined, I then refine the kinetic and plant-specific parameters in the SMB model, which are the mass transfer coefficients (k^{ma}) and the size of the dead volume (V_{dead}). These were treated as uncertain parameters in Steps 1-5, and their significant influence on the optimal operating conditions is shown in Figure 20. Each triangle represents one case among the 54 cases in Figure 20b, wherein the SMB model is optimized using the converged isotherm parameters while the mass transfer coefficients and the dead volume are varied. However, these model parameters can be accurately determined only by carrying out experiments using the SMB mini-plant and fitting the model to the experimental data. I first carried out two experimental runs (Runs *1-i* and *1-ii*) as summarized in Table 7 and Table 8. In each SMB experiment, I collected samples from the extract, raffinate, and the sampling points between each column at the end of the run (Step 6). SMB Run I was predicted by the base case (all mass transfer coefficients were set to be 1 min^{-1}, dead volume was set to be 0) using the converged isotherm from Step 5. It can be observed from Table 8 that the purity was lower than the initial prediction while the recovery was higher. I suspected that the mismatch was due to the effect of dead volume in the SMB mini-plant. Dead volume causes a delay of the liquid transport, thus delaying propagation of the concentration profiles. To compensate for the effect of the dead volume, the step time was increased in further experimental testing. In SMB Run *1-ii*, the step time was increased from 145 seconds to 160 seconds. I observed that while the purity increased, the recovery dropped significantly (Table 8). Figure 20b also shows that the operating conditions of the two runs are quite different. The experimental data from these two runs creates the basis for applying the *Steps 6-7* shown in Figure 14, to refine the remaining model parameters and improve the predictions.

Table 7 - SMB Operating Conditions.

Iteration *m*	Run	t_{st} [sec]	F_1 $[\frac{ml}{min}]$	F_2 $[\frac{ml}{min}]$	F_3 $[\frac{ml}{min}]$	F_4 $[\frac{ml}{min}]$
1	*1-i*	145	6	3.26	4.92	4
2	*1-ii*	160	6	3.26	4.92	4

In *Step 7*, the data from the first two SMB runs was used to refine the mass transfer coefficients and dead volume parameters, with the isotherm parameters fixed. This approach has been used in other reports where SMB model parameters are adjusted to fit experimental results [65, 66]. Table S7 shows the fitted values. With these updated parameters, the SMB model gave the optimal prediction shown in Table 7 (Run *2*). This operating condition is between Runs *1-i* and *1-ii* (Table 7) as explained by the triangle theory; the optimized model gave operating conditions intermediate between Run *1-i* (low purity and high recovery) and Run *1-ii* (high purity and low recovery). Run *2* was then performed experimentally (Table 8), and the results are in good agreement with the model prediction. The purity and recovery are very close to the model prediction. Figure 21 shows the model predictions (with the final parameter set) of the concentration profile and the corresponding experimental results for each of the three runs. A clear improvement in the matching of the predicted and experimental concentration profiles is seen for Run *2* as compared to Runs *1-i* and *1-ii*.

Table 8 - SMB experimental and model simulation results showing the toluene purity and recovery in the extract.

		Toluene purity			**Toluene recovery**		
ITER	Run	Model before fitting (%)	Model after fitting Run 1-i and 1-ii (%)	Experiment (%)	Model before fitting (%)	Model after fitting Run 1-I and 1-ii(%)	Experiment (%)
1	***1-i***	90.0	82.2	79.6	90.0	98.8	99.1
	1-ii	66.4	92.5	89.1	56.9	68.4	54.1
2	***2***	97.8	90.0	88.5	66.1	90.0	89.6

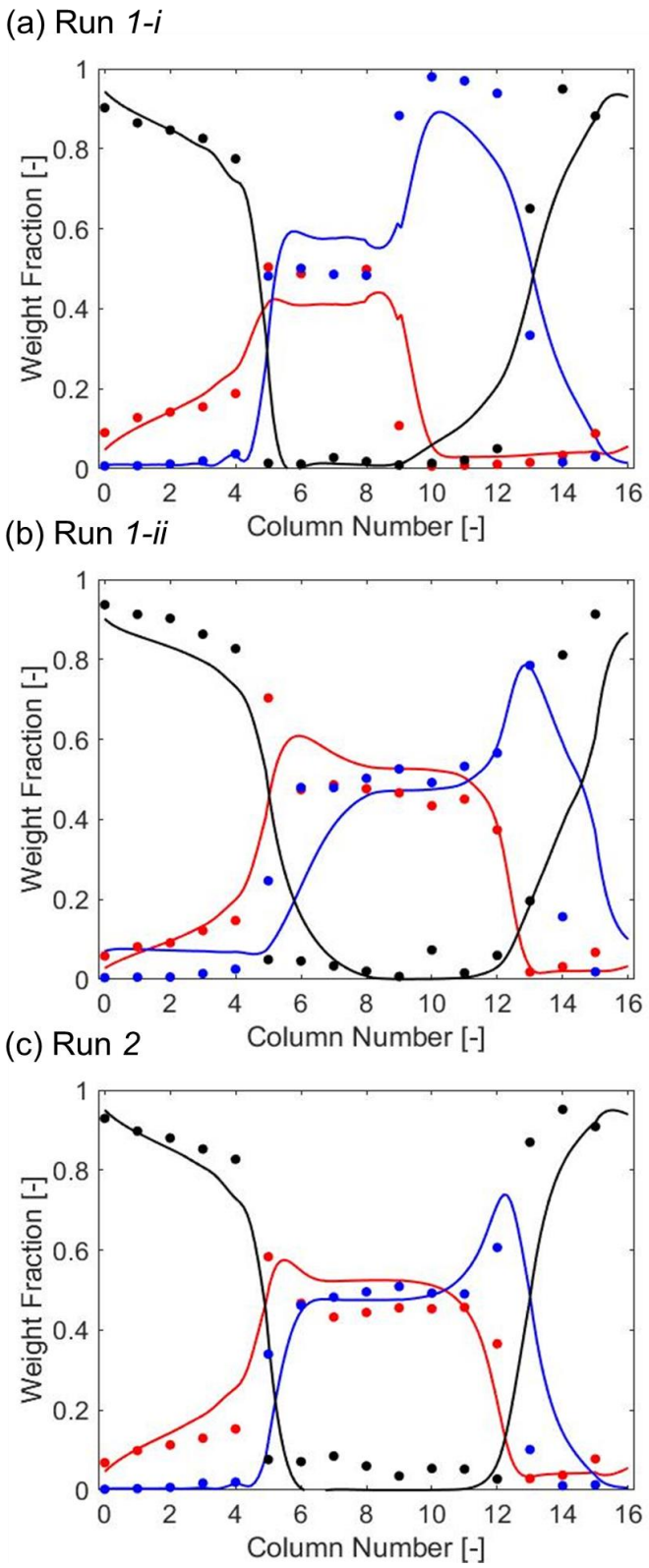

Figure 21 - Comparison of measured internal concentrations in SMB experiments (symbols) and predictions (curves) of the SMB model with the final set of parameters.

4.5 Conclusions

In this work, I have shown the application of a concurrent approach to determine an isotherm model and design an SMB process for aromatic/alkane separation, with a ternary toluene-dodecane-cyclohexane model system. In this approach, liquid mixture compositions were selected based on model predictions of the SMB concentration profile. I were able to converge the isotherm modeling with 33 multicomponent breakthrough experiments. The obtained final isotherm was used in the SMB model to predict optimal operating conditions. After appropriately fitting the mass transfer coefficients and system dead volume using additional experimental SMB data, I successfully demonstrated the experimental validation of toluene/dodecane separation with the desired specification in a 16-column SMB mini-plant constructed at Georgia Tech. The concurrent approach thus enabled us to achieve rapid process design while determining isotherm parameters, *i.e.,* no prior knowledge of the adsorption behavior is required.

The composition selection algorithm can be generalized to more than three components wherein it is expected to reduce the number of experimental measurements required greatly. Because the concurrent approach intrinsically selects compositions in a range that is most relevant to the operating conditions, it also enables the use of a simple isotherm model such as the multicomponent Langmuir isotherm, whose parameters are refined to provide sufficiently accurate predictions in the relevant region. The present work also shows the applicability of this method to challenging cases in which the feed mixture is supplied without dilution, so that all three components compete significantly for adsorption. Finally, the present approach allowed us to limit the SMB mini-plant runs to only three, at which point I obtained the target purity and recovery of the desired product (toluene) in the extract.

CHAPTER 5. MULTICOMPONENT PARTITIONING AT HIGH TEMPERATURE USING SIMULATED MOVING BED PROCESSES

5.1 Motivation

In this short Chapter, the concurrent approach demonstrated in the previous chapters is extended – at least in principle - to a new application at a higher temperature, which is a real condition in industrial-scale separations. Additional components (n-octane, 2-methylnaphthalene, and 1-phenyl dodecane) were included in the feed mixture that was used in Chapter 4. The separation goal is revised to partition the aromatic compounds and aliphatic compounds, and the first two iterations were carried out (iteration 0, and iteration 1). The operating condition is set to 150 ^{o}C, which is a more practical condition to avoid slow mass transfer resistance but is more challenging for SMB operations.

5.2 Methodology

Unless explicitly stated, the methods are the same as the previous work. The concurrent approach (Figure 5) was followed again. Although I have some information on the adsorption of toluene, dodecane, and cyclohexane at room temperature, I expected the adsorption behavior would change at 150 ^{o}C. Therefore, a few compositions were selected randomly to initialize the concurrent approach. The SMB modeling was the same except a few more components (n-octane, 2-methylnaphthalene, and 1-phenyl dodecane) were included. The experimental apparatus was unchanged as well except that the column oven was maintained at 150 ^{o}C instead of at room temperature. The same methods were used for data analysis for breakthrough results and GC

results. The adsorbent used in this study was still silica gel (Davisil Grade 923). Procedures for preparing the packed column were the same.

5.3 Results and Discussion

Table 9 shows the liquid compositions tested for isotherm determination, and

Table 11 shows the corresponding experimental results. After completing the experimental study in each iteration, isotherm parameters were calculated using the same approach stated in Chapter 3, section 3.2.2. The obtained isotherm parameters were shown in Table 13, and selectivity (Table 14) was calculated based on the isotherm parameters. The predicted SMB concentration profiles were shown in Figure 22. These results were analyzed based on iterations in the following detailed discussion.

Table 9 – Tested liquid compositions

Experiments	ITER	Toluene	Dodecane	Cyclohexane	n-Octane	1-Phenyl-dodecane	2-Methyl-Naphthalene
1	0	0.0%	0.0%	100.0%	0.0%	0.0%	0.0%
2		0.0%	100.0%	0.0%	0.0%	0.0%	0.0%
3		100.0%	0.0%	0.0%	0.0%	0.0%	0.0%
4		0.0%	0.0%	0.0%	100.0%	0.0%	0.0%
5		0.0%	0.0%	0.0%	0.0%	100.0%	0.0%
6		33.8%	0.0%	0.0%	66.2%	0.0%	0.0%
7		0.0%	0.0%	15.1%	0.0%	84.9%	0.0%
8		0.0%	0.0%	52.4%	0.0%	0.0%	47.6%
9		0.0%	85.4%	0.0%	0.0%	0.0%	14.6%
10		0.0%	0.0%	0.0%	0.0%	89.4%	10.6%
11		0.0%	0.0%	38.8%	61.2%	0.0%	0.0%
12		0.0%	69.5%	0.0%	30.5%	0.0%	0.0%
13		64.0%	0.0%	36.0%	0.0%	0.0%	0.0%
14		34.8%	65.2%	0.0%	0.0%	0.0%	0.0%
15		65.1%	0.0%	0.0%	0.0%	34.9%	0.0%
16		0.0%	43.8%	56.2%	0.0%	0.0%	0.0%
17		0.0%	77.8%	0.0%	0.0%	22.2%	0.0%
18		0.0%	0.0%	0.0%	79.6%	20.4%	0.0%

Table 10 continued – Tested liquid compositions

Experiments	ITER	Toluene	Dodecane	Cyclohexane	n-Octane	1-Phenyl-dodecane	2-Methyl-Naphthalene
19		63.4%	0.0%	0.0%	0.0%	0.0%	36.6%
20		0.0%	0.0%	0.0%	80.3%	0.0%	19.7%
21		0.2%	0.0%	99.7%	0.0%	0.0%	0.1%
22	1	6.9%	0.8%	77.6%	0.6%	8.2%	6.0%
23		11.5%	3.2%	55.3%	2.2%	17.4%	10.5%
24		14.2%	6.8%	37.1%	4.0%	24.6%	13.3%
25		15.4%	10.3%	24.5%	5.9%	29.3%	14.6%
26		16.0%	15.1%	12.9%	8.0%	32.7%	15.4%
27		15.7%	20.8%	4.0%	10.2%	34.1%	15.2%
28		9.6%	28.0%	1.4%	12.6%	37.3%	11.2%
29		5.7%	32.4%	7.0%	14.4%	33.2%	7.3%
30		3.7%	34.7%	14.9%	15.0%	26.8%	4.9%
31		2.5%	34.3%	25.0%	14.3%	20.6%	3.4%
32		1.5%	30.3%	40.8%	11.9%	13.5%	2.0%
33		0.9%	22.8%	58.7%	8.5%	7.9%	1.1%

Table 11 – Experimental results from breakthrough experiments, unit: g/g_{ads}

EXP	Iterations	Toluene	Dodecane	Cyclohexane	n-Octane	1-Phenyl-dodecane	2-Methyl-Naphthalene
1	0	0.000	0.000	0.305	0.000	0.000	0.000
2		0.000	0.359	0.000	0.000	0.000	0.000
3		0.371	0.000	0.000	0.000	0.000	0.000
4		0.000	0.000	0.000	0.285	0.000	0.000
5		0.000	0.000	0.000	0.000	0.469	0.000
6		0.136	0.000	0.000	0.165	0.000	0.000
7		0.000	0.000	0.063	0.000	0.383	0.000
8		0.000	0.000	0.182	0.000	0.000	0.245
9		0.000	0.268	0.000	0.000	0.000	0.102
10		0.000	0.000	0.000	0.000	0.400	0.063
11		0.000	0.000	0.108	0.162	0.000	0.000
12		0.000	0.225	0.000	0.096	0.000	0.000
13		0.244	0.000	0.103	0.000	0.000	0.000
14		0.144	0.176	0.000	0.000	0.000	0.000
15		0.255	0.000	0.000	0.000	0.113	0.000
16		0.000	0.157	0.193	0.000	0.000	0.000
17		0.000	0.295	0.000	0.000	0.125	0.000
18		0.000	0.000	0.000	0.228	0.094	0.000

Table 12 continued – Experimental results from breakthrough experiments, unit: g/g_{ads}

EXP	Iterations	Toluene	Dodecane	Cyclohexane	n-Octane	1-Phenyl-dodecane	2-Methyl-Naphthalene
19		0.258	0.000	0.000	0.000	0.000	0.150
20		0.000	0.000	0.000	0.227	0.000	0.109
21		0.001	0.000	0.301	0.000	0.000	0.001
22	1	0.031	0.002	0.245	0.002	0.020	0.031
23		0.050	0.011	0.177	0.006	0.054	0.058
24		0.065	0.018	0.135	0.012	0.057	0.065
25		0.073	0.029	0.094	0.019	0.071	0.074
26		0.077	0.046	0.051	0.027	0.087	0.081
27		0.088	0.062	0.014	0.033	0.086	0.075
28		0.051	0.089	0.005	0.045	0.104	0.062
29		0.031	0.099	0.028	0.051	0.096	0.042
30		0.020	0.101	0.061	0.053	0.072	0.031
31		0.013	0.099	0.094	0.046	0.059	0.021
32		0.008	0.080	0.146	0.036	0.036	0.013
33		0.005	0.060	0.198	0.024	0.022	0.007

Table 13 – Isotherm parameters.

	Iteration 0		Iteration 1	
	k^{eq} [cm³/g]	Q^{sat} [g/cm³]	k^{eq} [cm³/g]	Q^{sat} [g/cm³]
1-Phenyl Dodecane	1012	0.533	1110	0.527
2-Metyhl Naphthalene	1000	0.579	1032	0.563
Cyclohexane	1331	0.361	1209	0.342
Dodecane	1057	0.405	1158	0.402
n-Octane	1400	0.322	1412	0.320
Toluene	1410	0.417	1340	0.414

Table 14 – Selectivity calculated from isotherm parameters

	Iteration 0	Iteration 1
Toluene/1-Phenyl Dodecane	1.090	1.005
Toluene/2-Metyhl Naphthalene	1.015	1.012
Toluene/Cyclohexane	1.224	1.422
Toluene/Dodecane	1.373	1.263
Toluene/n-Octane	1.304	1.301

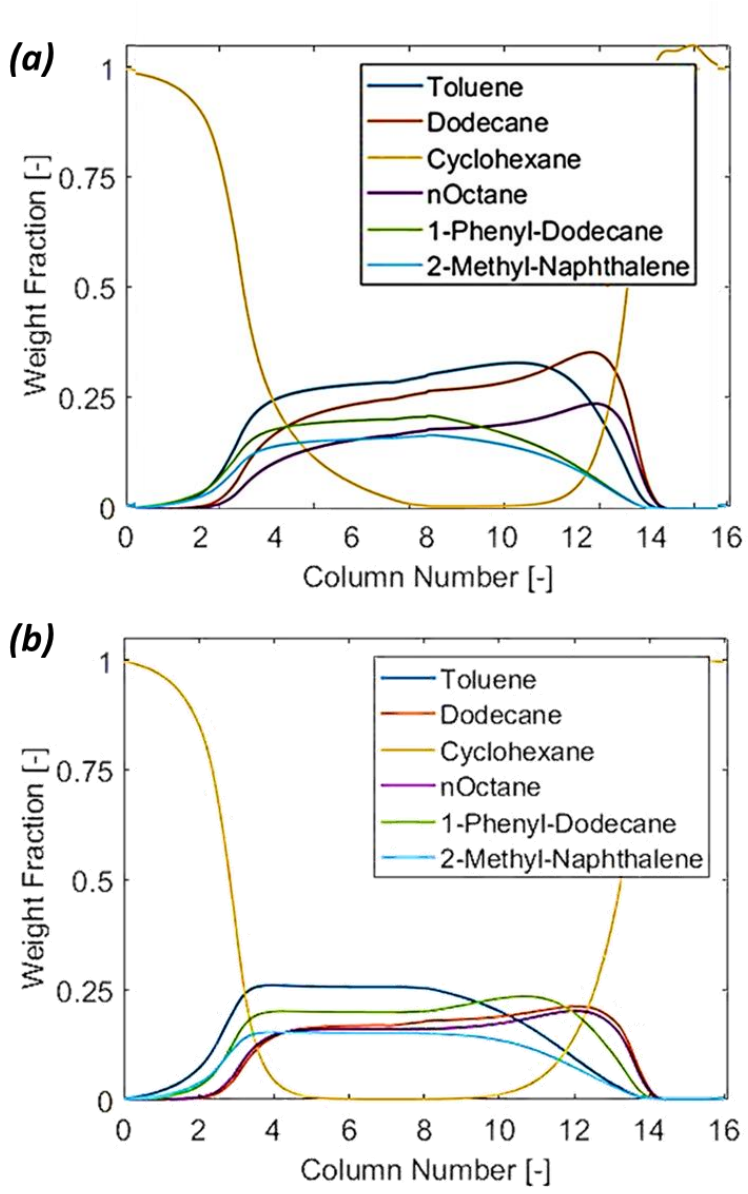

Figure 22 - Concentration Profiles. (a) Optimal SMB operation concentration profile predicted based on isotherm parameters in iteration 0; (b) Optimal SMB operation concentration profile predicted based on isotherm parameters in iteration 1.

5.3.1 Iteration 0

The iterations of the concurrent approach still start with a random selection of liquid compositions for breakthrough experiments. Composition 1-21 in Table 9 were liquid compositions tested in iteration 0. It can be easily observed from Table 14 that the selectivity of

the aromatic compounds was low (about 1.0), but the selectivity between aromatics and aliphatic was significantly higher (about 1.3). In this study, the SMB separation was designed to separate aromatic compounds and aliphatic compounds.

The SMB operation was optimized based on the isotherm parameters in iteration 0, and the concentration profile is shown in Figure 22a. The SMB process was optimized for maximum productivity under two process constraints: purity of aromatic compounds in the extract higher than 80% and the purity of the aliphatic compounds in the raffinate higher than 80%. Here, the purity constraints ($\geq$ 80%) were chosen arbitrarily. I confirmed that a higher purity can be achieved by the model optimization. However, to achieve such a high purity, the desorbent-to-feed ratio exceeds 120, which is too high for the process to be realistically operated.

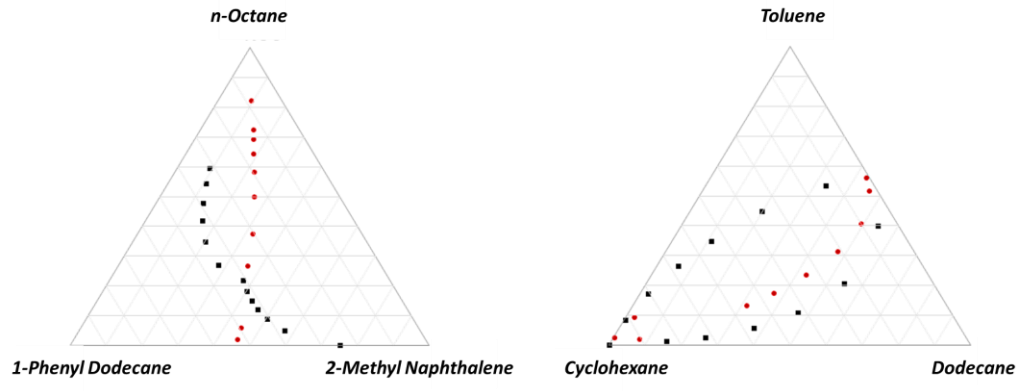

Figure 23 – Selected Liquid Compositions. Black: compositions selected in iteration 1; Red: compositions selected in iteration 2. Compositions selected in iteration 0 was not shown on this plot.

5.3.2 *Iteration 1*

The new iteration starts with compositions selection based on the concentration profile of the previous iteration. From the concentration profiles predicted in iteration 0, 12 liquid compositions were selected. Black squares in Figure 23 shows the compositions selected and tested in this iteration. To represent the 6 components, two ternary diagrams were used to visualize the selected compositions.

After the selected compositions were tested using breakthrough experiments, the obtained adsorption measurements were used to fit a new set of isotherm parameters. Again, model optimization was carried out based on the isotherm parameters, and the obtained concentration profile is shown in Figure 22b. The difference between the predicted concentration profile in iteration 0 and that in iteration 1 was observable, and hence a new iteration was carried out.

5.3.3 *Iteration 2*

10 more liquid compositions were selected to ensure the new concentration profile was modeled accurately. These liquid compositions were the red squares in Figure 23. It can be observed that there were no compositions tested redundantly in iteration 2 given iteration 1. For example, in the plot of toluene-cyclohexane-dodecane (Figure 23), the upper half of the concentration profile that was covered by experimental measurements in iteration 1 was not tested repeatedly.

5.4 **Conclusion**

The concurrent approach was extended to SMB separation with a larger number of components at a higher temperature. This study has also shown that when using the concurrent

approach, the SMB process design is not limited to the purification one particular component but can be applied to partitioning (or fractionating) a more complex mixture into two groups.

CHAPTER 6. CONCLUSION AND FUTURE WORK

6.1 Conclusions

The key achievements of my thesis research can be summarized in the following four points, and their detailed explanation follows.

1. A concurrent approach for simultaneous isotherm characterization and process optimization was developed.
2. In this concurrent approach, an algorithm was developed to select key liquid compositions based on model simulation.
3. By applying the concurrent approach, experimental effort for process development can be greatly reduced.
4. The results obtained using the concurrent approach was successfully validated on SMB mini-plant.

The development of the concurrent approach starts with the work on xylene separation. This approach was developed to study the competitive adsorption of the five-component mixture. The same approach was improved further when it was applied to the toluene-dodecane separation. In this project, the effect of the uncertainty of plant-specific parameters was considered. The isotherm developed was robust within reasonable ranges of mass transfer coefficients and SMB plant dead volumes.

The composition selection algorithm is a critical step in the proposed concurrent approach. All liquid compositions were treated as vectors with each element being the concentration. Concentration profiles obtained from SMB process model optimization and simulation were

stored as a set of vectors of liquid phase compositions. In this algorithm, the screening started with the first vector of the set; the vector was compared to all experimentally tested compositions. 2-norm (distance) was used to determine the similarity between vectors. Vectors that were significantly different from each other were collected, and liquid phase breakthrough experiments were carried out using those vector values as feed compositions.

A total of 23 experiments were done to establish an isotherm for xylene adsorption, which was a significant reduction of experimental efforts if compared to full factorial design. Similarly, only 33 experiments were needed to establish a robust isotherm for SMB model optimization.

The obtained SMB process optimization results were validated on an SMB mini-plant built in-house. When targeted with 90% purity and 90% recovery of toluene in the extract in model optimization, I obtained 88.5% purity and 89.6% recovery experimentally. The mismatch between experiments and model prediction was as small as 1.5%.

6.2 **Future work**

6.2.1 Further Generalization of the Concurrent Approach

It is interesting to further generalize the concurrent approach to a higher number of components in the feed. For xylene separation, there are more components in a realistic separation process. Xylene isotherms are the main components, but there are also some non-aromatics linear alkanes. These components do not retain on the zeolite and may breakthrough the buffer zone and contaminate the extract.

For toluene-dodecane separation, this system is often mixed with many other aromatic, and aliphatic compounds since the source of the feedstock may be the catalytic reforming process.

The product of the reforming process may contain up to 30 different compounds. It is an interesting and important separation because the compounds have overlapping boiling points making the efficient separation by distillation difficult [11]. Studying those components one-by-one is not an option due to the tremendous amount of experimental efforts. Using concurrent approach may lead to the rapid discovery of optimal process design.

6.2.2 Applying Concurrent Approach to PowerFeed/VariCol

The concurrent approach was developed for 4-zone SMB separation under constant flow rates and zone configurations. In PowerFeed SMB operation flow rates alternate between low and high to accommodate the cyclic nature of the SMB operation. In VariCol operation, inlet/outlet locations change individually leading to changing zone configurations at each step.

Applying the concurrent approach to PowerFeed and VariCol type separations can be done by considering the concentration profile at different temporal points. In the concurrent set-up, the concurrent approach was applied to the concentration profile at one temporal point. To generalize the concurrent approach to include the changes of concentration profile in the temporal domain will enable it to be applied to PowerFeed/VariCol operations.

APPENDIX A. SUPPORTING INFORMATION

A.1 Supporting Information for Xylene Separation Study (Chapter 3)

A.1.1 Retention Time in GC Method

Table A.1.1: Retention time of Xylenes and other aromatics

Component	Retention Time (min)
n-hexane	2.373
ethylbenzene	13.047
***p*-xylene**	13.438
***m*-xylene**	13.633
***o*-xylene**	15.302
***p*-diethylbenzene**	20.327
tri-isopropylbenzene	28.004

A.1.2 Adsorption Measurements

Table A.1.2: Experimental Results. Adsorbed mass (q^{eq}) was calculated by frontal analysis. Experiments: R1, R2, and R3 are the three reference experimental measurements.

Experiments	Liquid Compositions [%]					Adsorbed mass [g-component/g-adsorbent]				
	p-xylene	*m*-xylene	*o*-xylene	Ethyl benzene	*p*-diethyl benzene	*p*-xylene	*m*-xylene	*o*-xylene	Ethyl benzene	*p*-diethyl benzene
1	22.1	0.3	0.2	0.1	75.1	0.024	0.000	0.000	0.000	0.060
2	38.8	0.3	0.2	0.1	58.4	0.045	0.000	0.000	0.000	0.042
3	48.5	0.1	0.0	0.0	49.2	0.055	0.000	0.000	0.000	0.031
4	58.4	10.0	5.3	5.2	19.6	0.063	0.007	0.005	0.004	0.009
5	0.1	29.7	14.6	14.6	38.4	0.000	0.029	0.016	0.014	0.039
6	0.0	19.8	9.7	9.8	58.3	0.000	0.015	0.009	0.008	0.058
7	51.0	12.0	0.9	22.6	12.4	0.059	0.008	0.001	0.016	0.006
8	28.2	26.9	2.7	33.4	7.8	0.040	0.021	0.003	0.024	0.005
9	20.6	45.5	9.7	19.3	3.9	0.030	0.039	0.010	0.012	0.002
10	3.7	49.2	13.0	15.1	18.0	0.006	0.047	0.014	0.012	0.014
11	17.9	33.8	8.1	16.6	22.0	0.025	0.027	0.008	0.013	0.015
12	0.0	9.8	4.8	4.8	78.2	0.000	0.006	0.004	0.004	0.067
13	0.1	0.6	0.2	0.1	96.4	0.000	0.000	0.000	0.000	0.091
14	26.6	8.1	6.8	2.2	54.0	0.034	0.006	0.007	0.002	0.042
15	24.8	17.8	9.0	4.9	41.4	0.034	0.015	0.009	0.004	0.030
16	17.6	5.1	5.0	1.0	68.8	0.020	0.004	0.005	0.001	0.054
17	11.7	0.0	0.0	0.0	86.0	0.013	0.000	0.000	0.000	0.078
18	5.0	41.0	14.3	12.1	24.9	0.009	0.040	0.016	0.010	0.019

Table A.1.2 continued: Experimental Results. Adsorbed mass (q^{eq}) was calculated by frontal analysis. Experiments: R1, R2, and R3 are the three reference experimental measurements.

Experiments	Liquid Compositions [%]					Adsorbed mass [g-component/g-adsorbent]				
	p-xylene	*m*-xylene	*o*-xylene	Ethyl benzene	*p*-diethyl benzene	*p*-xylene	*m*-xylene	*o*-xylene	Ethyl benzene	*p*-diethyl benzene
19	17.7	24.8	17.8	6.2	31.3	0.025	0.020	0.017	0.005	0.021
20	13.5	32.5	11.8	8.8	31.2	0.020	0.027	0.011	0.007	0.021
21	1.0	34.0	10.4	8.6	43.7	0.001	0.029	0.010	0.007	0.040
22	0.0	19.9	4.8	5.8	67.3	0.000	0.014	0.004	0.005	0.064
R1	0.6	0.9	0.2	46.6	48.8	0.000	0.000	0.000	0.037	0.058
R2	0.1	0.2	51.2	0.4	45.3	0.000	0.000	0.041	0.000	0.053
R3	0.0	45.1	0.4	50.6	0.2	0.000	0.052	0.000	0.049	0.000

A.1.2 Sieve Degradation

The experimental setup was identical to Figure 4. A 50:50 (volume) mixture of xylene and PDEB (Table S3) was supplied to the packed BaX column at 180 ^{o}C. To measure the adsorption capacity of the fresh molecular sieve, five breakthrough experiments were carried out on the fresh BaX column shown as the first six data points on *Figure S1* (include the analysis on the reverse breakthrough curve of the first experiment). The liquid volume supplied to the BaX column for one breakthrough experiment was estimated to be around 3 to 4 bed volumes. The goal of running several breakthrough experiments continuously was to establish a baseline of adsorption properties. After this initial testing, the same mixture was supplied to the column continuously and breakthrough experiments were carried out approximately every 50 bed-volumes of cumulative liquid volume.

Table A.1.3: liquid mixture used for sieves degradation study

***p*-xylene**	***m*-xylene**	***o*-xylene**	**Ethylbenzene**	***p*-Diethyl benzene**
11.8	24.5	6.4	7.0	50.0

As shown in *Figure S1*, when the same column was repeatedly tested, its performance slowly decreased over time. Up to a total liquid volume of about 100 bed volumes, the degradation seems to be within the margin of experimental error. However, when additional liquid mixture was supplied to the column, the capacity starts to decrease slowly. The experimental error of sieve capacity is estimated to be around 5%, similar experimental error was present when calculating selectivity (*Figure S2).*

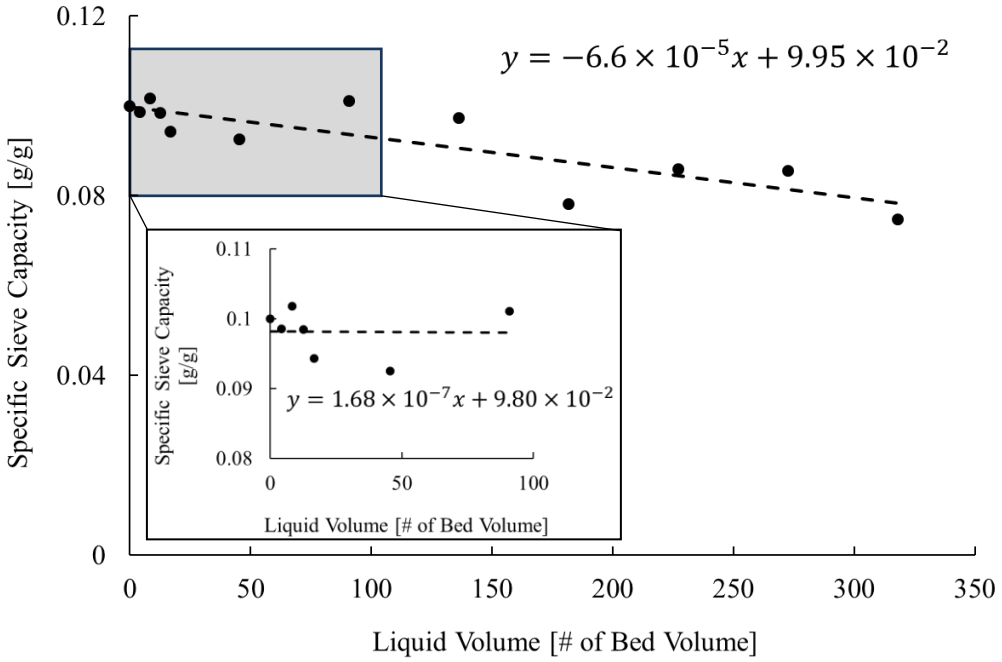

Figure A.1.1: Experimental accuracy and performance degradation

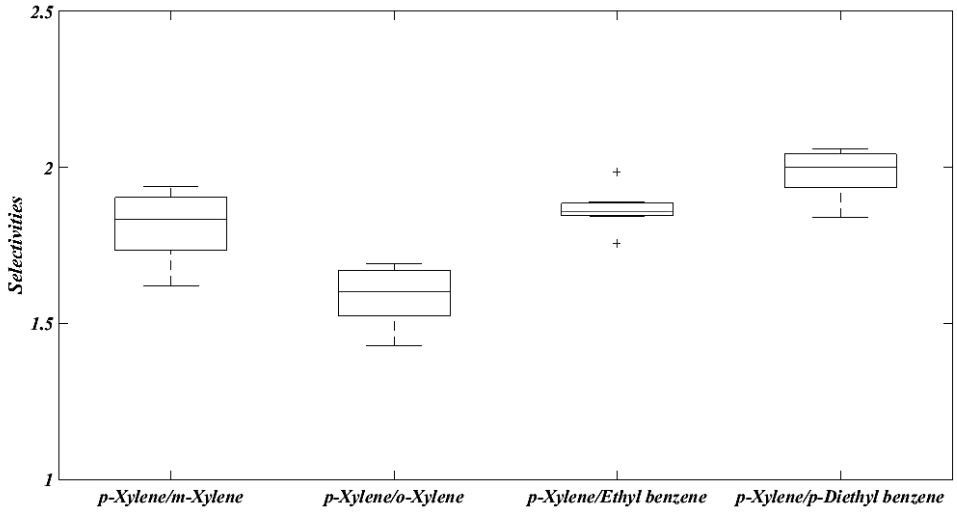

Figure A.1.2: Experimental accuracy of sieves selectivity within 100 bed volumes

A.2 Supporting Information for Toluene-Dodecane Separation Study (Chapter 4)

A.2.1 Uncertain Parameters

Table A.2.15: Values of mass transfer and dead volume parameters used composition selection.

Dead volume **[%]**	$k^{ma}_{toluene}$ **[min^{-1}]**	$k^{ma}_{dodecane}$ **[min^{-1}]**	$k^{ma}_{cyclohexane}$ **[min^{-1}]**
0.0 and 2.5	0.5, 1.0 and 2.0	0.5, 1.0 and 2.0	0.5, 1.0 and 2.0

A.2.2 Adsorption Measurements

Table A.2.2: Liquid compositions and experimental results.

		Feed Composition (mass fraction, dimensionless)			Adsorbed Mass (g/g_{ads})		
		Toluene (%)	Dodecane (%)	Cyclohexane (%)	Toluene	Dodecane	Cyclohexane
$k = 0$	1	33.3	33.3	33.4	0.1396	0.0119	0.0311
	2	50.0	0	50.0	0.1624	0.0000	0.0427
	3	0	50.0	50.0	0.0000	0.0716	0.0848
	4	100.0	0	0	0.2402	0.0000	0.0000
	5	0	100.0	0	0.0000	0.1846	0.0006
	6	0	0	100.0	0.0000	0.0000	0.1612
	7	14.0	14.0	73.0	0.0940	0.0068	0.1807
$k = 1$	8	16.0	58.0	26.0	0.1141	0.0550	0.0452
	9	54.0	16.0	30.0	0.1697	0.0100	0.0337
	10	55.0	39.0	6.0	0.1920	0.0313	0.0027
	11	33.0	64.0	3.0	0.1789	0.0757	0.0044
	12	24.0	76.0	0	0.1124	0.0684	0.0000
	13	41.0	7.0	52.0	0.1449	0.0023	0.0430
	14	4.0	45.0	51.0	0.0561	0.0623	0.0914
	15	2.0	23.0	75.0	0.0340	0.0265	0.1110
	16	1.0	0	99.0	0.0211	0.0000	0.1498
$k = 2$	17	32.0	1.0	67.0	0.1365	0.0010	0.0509
	18	53.0	6.0	41.0	0.1714	0.0041	0.0320
	19	60.0	25.0	15.0	0.1907	0.0205	0.0118
	20	47.0	51.0	2.0	0.1362	0.0494	0.0001
	21	24.0	63.0	13.0	0.1208	0.0497	0.0098
	22	4.0	58.0	38.0	0.0575	0.0623	0.0501
	23	3.0	34.0	63.0	0.0386	0.0402	0.0899
$k = 3$	24	2.0	11.0	87.0	0.0280	0.0163	0.1269
	25	8.0	0	92.0	0.0616	0.0000	0.1359
	26	16.0	0	84.0	0.0900	0.0001	0.0959

Table A.2.2 continued: Liquid compositions and experimental results.

	Feed Composition (mass fraction, dimensionless)			Adsorbed Mass (g/g_{ads})		
	Toluene (%)	Dodecane (%)	Cyclohexane (%)	Toluene	Dodecane	Cyclohexane
27	23.0	0	77.0	0.1029	0.0000	0.0813
28	45.0	10.0	45.0	0.1474	0.0057	0.0338
29	51.0	25.0	24.0	0.1660	0.0411	0.0278
30	52.0	32.0	16.0	0.1762	0.0224	0.0157
31	38.0	56.0	6.0	0.1680	0.0360	0.0076
32	17.0	70.0	13.0	0.1175	0.0645	0.0188
33	13.0	66.0	21.0	0.1752	0.0224	0.0161

A.2.3 Plant Specific Parameter Estimation

In Step 8 of the proposed algorithm, the mass transfer coefficients and dead volume are estimated from the internal compositions sampled from the SMB experiments. The estimation is carried out in a similar manner as in Step 3, where a regularization term was added to the objective function as shown in Table S6. The model equation used in Step 4 (equality constraints in Table S5) was used as equality constraints.

Table A.2.3: Model formulation for parameter fitting, where φ is the objective function, i is the index for liquid components (toluene, dodecane, or cyclohexane), n is the index for columns, j is the index that iterate through all decision variables. $C_{i,n}^{exp}$ is the internal liquid concentration of component i of column n measured in SMB experiments, and $C_{i,n}^{model}$ is the liquid concentration of component i of column n predicted by SMB process model. M′ is the parameter for the regularization term.

Objective function	$\min \varphi_k^{leastSquare} = \sum_{\substack{i=1 \\ n=1}}^{\substack{N_{comp} \\ N_{measure}}} \left(\left(C_{i,n}^{exp} - C_{i,n}^{model} \right)^2 \right) + M' \cdot \sum_j \left(\frac{\theta_j - \theta_j^0}{\theta_j^0} \right)^2$
Decision variables	$\theta_j = k_{toluene}, k_{dodecane}, k_{cyclohexane}, V_{dead}$
Constraints	All equality constraints in Table S5.

The fitted parameter values were within the consideration of our perdition of the range of uncertainty (Table S7). The regularization term $M' \cdot \sum_j \left(\frac{\theta_j - \theta_j^0}{\theta_j^0} \right)^2$ in the objective function (Table S6) prevented the parameter values deviate too much from the initial values. Mass transfer values for all components were simulated within the range of 0.5 min^{-1} to 2 min^{-1} and the value of 1.6 min^{-1} to 1.8 min^{-1} were within the range of initial estimation.

Table A.2.4: Values of mass transfer coefficients and dead volume parameters.

Parameter	Initial	Fitted
$k_{cyclohexane}$	1.0 min^{-1}	1.7 min^{-1}
$k_{dodecane}$	1.0 min^{-1}	1.8 min^{-1}
$k_{toluene}$	1.0 min^{-1}	1.6 min^{-1}
V_{dead}	0 ml/column	0.31 ml/column

REFERENCESREFERENCES

[1] MINCEVA, M. and A. E. RODRIGUES, "Modeling and simulation of a simulated moving bed for the separation of p-xylene," Industrial & Engineering Chemistry Research, 2002. 41(14): p. 3454-3461.

[2] AZEVEDO, D. and A. E. RODRIGUES, "Fructose–glucose separation in a SMB pilot unit: modeling, simulation, design, and operation," AIChE journal, 2001. 47(9): p. 2042-2051.

[3] NAGAMATSU, S., K. MURAZUMI, and S. MAKINO, "Chiral separation of a pharmaceutical intermediate by a simulated moving bed process1," Journal of Chromatography A, 1999. 832(1-2): p. 55-65.

[4] GUEST, D. W., "Evaluation of simulated moving bed chromatography for pharmaceutical process development," Journal of Chromatography A, 1997. 760(1): p. 159-162.

[5] WILLIAM, D. J., "Perfumes cosmetics, perfumed soaps, essences, and analogous preparations". 1935, Google Patents.

[6] PÉREZ-FERNÁNDEZ, V., et al., "Separation of phthalates by cyclodextrin modified micellar electrokinetic chromatography: Quantitation in perfumes," Analytica chimica acta, 2013. 782: p. 67-74.

[7] NIESSEN, W., "Analysis of antibiotics by liquid chromatography–mass spectrometry," Journal of Chromatography A, 1998. 812(1-2): p. 53-75.

[8] MASON, D. M., "Isolation of xylene isomers". 1950, Google Patents.

[9] HOFF, M. C. and K. C. PETERSON, "Separation of recovery of xylene isomers". 1957, Google Patents.

[10] EGAN, C. J. and R. V. LUTHY, "Separation of xylenes," Industrial & Engineering Chemistry, 1955. 47(2): p. 250-253.

[11] MEYERS, R. A. and P. J. SILADY, *Handbook of petroleum refining processes*. Vol. 548. 2004: McGraw-Hill New York.

[12] HAGNAUER, G. L., "Size exclusion chromatography," Analytical Chemistry, 1982. 54(5): p. 265-276.

[13] HEMSTRÖM, P. and K. IRGUM, "Hydrophilic interaction chromatography," Journal of Separation Science, 2006. 29(12): p. 1784-1821.

[14] JUNGBAUER, A. and R. HAHN, *Chapter 22 Ion-Exchange Chromatography*, in *Methods in Enzymology*, R.R. Burgess and M.P. Deutscher, Editors. 2009, Academic Press. p. 349-371.

[15] SCHMIDT-TRAUB, H., *Preparative chromatography: of fine chemicals and pharmaceutical agents*. 2006: John Wiley & Sons.

[16] RUTHVEN, D. M. and C. B. CHING, "Counter-current and simulated counter-current adsorption separation processes," Chemical Engineering Science, 1989. 44(5): p. 1011-1038.

[17] NEUZIL, R. W. and A. J. DE ROSSET, "Olefin separation process". 1970, Google Patents.

[18] STORTI, G., et al., "Robust design of binary countercurrent adsorption separation processes," AIChE Journal, 1993. 39(3): p. 471-492.

[19] AGRAWAL, G. and Y. KAWAJIRI, "Comparison of various ternary simulated moving bed separation schemes by multi-objective optimization," Journal of Chromatography A, 2012. 1238: p. 105-113.

[20] AGRAWAL, G., B. SREEDHAR, and Y. KAWAJIRI, "Systematic optimization and experimental validation of ternary simulated moving bed chromatography systems," J Chromatogr A, 2014. 1356: p. 82-95.

[21] MAZZOTTI, M., G. STORTI, and M. MORBIDELLI, "Robust Design of Countercurrent Adsorption Separation Processes .2. Multicomponent Systems," Aiche Journal, 1994. 40(11): p. 1825-1842.

[22] MAZZOTTI, M., G. STORTI, and M. MORBIDELLI, "Robust design of countercurrent adsorption separation .3. Nonstoichiometric systems," Aiche Journal, 1996. 42(10): p. 2784-2796.

[23] MAZZOTTI, M., G. STORTI, and M. MORBIDELLI, "Robust design of countercurrent adsorption separation processes .4. Desorbent in the feed," Aiche Journal, 1997. 43(1): p. 64-72.

[24] MIGLIORINI, C., M. MAZZOTTI, and M. MORBIDELLI, "Robust design of countercurrent adsorption separation processes: 5. Nonconstant selectivity," Aiche Journal, 2000. 46(7): p. 1384-1399.

[25] MAZZOTTI, M., G. STORTI, and M. MORBIDELLI, "Optimal operation of simulated moving bed units for nonlinear chromatographic separations," Journal of Chromatography A, 1997. 769(1): p. 3-24.

[26] BIEGLER, L. T. and V. M. ZAVALA, "Large-scale nonlinear programming using IPOPT: An integrating framework for enterprise-wide dynamic optimization," Computers & Chemical Engineering, 2009. 33(3): p. 575-582.

[27] KAWAJIRI, Y. and L. T. BIEGLER, "Nonlinear programming superstructure for optimal dynamic operations of simulated moving bed processes," Industrial & Engineering Chemistry Research, 2006. 45(25): p. 8503-8513.

[28] GUIOCHON, G. and O. TRAPP, "Basic principles of chromatography," Ullmann's Encyclopedia of Industrial Chemistry, 2012.

[29] RUTHVEN, D. M., *Principles of adsorption and adsorption processes*. 1984: John Wiley & Sons.

[30] LUDEMANN-HOMBOURGER, O., M. BAILLY, and R. M. NICOUD, "Design of a simulated moving bed: Optimal particle size of the stationary phase," Separation Science and Technology, 2000. 35(9): p. 1285-1305.

[31] GLUECKAUF, E. and J. COATES, "241. Theory of chromatography. Part IV. The influence of incomplete equilibrium on the front boundary of chromatograms and on the effectiveness of separation," Journal of the Chemical Society (Resumed), 1947: p. 1315-1321.

[32] BIEGLER, L. T., I. E. GROSSMANN, and A. W. WESTERBERG, "Systematic methods for chemical process design," 1997.

[33] CHUE, K., et al., "Comparison of activated carbon and zeolite 13X for CO2 recovery from flue gas by pressure swing adsorption," Industrial & Engineering Chemistry Research, 1995. 34(2): p. 591-598.

[34] KAWAJIRI, Y. and L. T. BIEGLER, "Optimization strategies for simulated moving bed and PowerFeed processes," AIChE journal, 2006. 52(4): p. 1343-1350.

[35] BIEGLER, L. T., *Nonlinear programming: concepts, algorithms, and applications to chemical processes*. Vol. 10. 2010: Siam.

[36] BUTLER, J. and C. OCKRENT, "Studies in electrocapillarity. III," The Journal of Physical Chemistry, 1930. 34(12): p. 2841-2859.

[37] CHOY, K. K., J. F. PORTER, and G. MCKAY, "Langmuir isotherm models applied to the multicomponent sorption of acid dyes from effluent onto activated carbon," Journal of Chemical & Engineering Data, 2000. 45(4): p. 575-584.

[38] MINCEVA, M. and A. E. RODRIGUES, "Adsorption of xylenes on faujasite-type zeolite - Equilibrium and kinetics in batch adsorber," Chemical Engineering Research & Design, 2004. 82(A5): p. 667-681.

[39] TOURNIER, H., et al., "Adsorption equilibrium of xylene isomers and p-diethylbenzene on a prehydrated BaX zeolite," Industrial & Engineering Chemistry Research, 2001. 40(25): p. 5983-5990.

[40] BELLAT, J.-P. and M.-H. SIMONOT-GRANGE, "Adsorption of gaseous p-xylene and m-xylene on NaY, KY, and BaY zeolites. Part 2: Modeling. Enthalpies and entropies of adsorption," Zeolites, 1995. 15(3): p. 219-227.

[41] TALU, O. and I. ZWIEBEL, "Multicomponent adsorption equilibria of nonideal mixtures," AIChE Journal, 1986. 32(8): p. 1263-1276.

[42] TOURNIER, H., et al., "Two experimental methods to study adsorption equilibria of xylene isomers in the liquid phase on a Y zeolite," Microporous and mesoporous materials, 2000. 39(3): p. 537-547.

[43] TALU, O., C. J. GUO, and D. T. HAYHURST, "Heterogeneous Adsorption Equilibria with Comparable Molecule and Pore Sizes," Journal of Physical Chemistry, 1989. 93(21): p. 7294-7298.

[44] LACHET, V., et al., "Molecular simulation of p-xylene and m-xylene adsorption in Y zeolites. Single components and binary mixtures study," Langmuir, 1999. 15(25): p. 8678-8685.

[45] COTTIER, V., et al., "Adsorption of p-xylene/m-xylene gas mixtures on BaY and NaY zeolites. Coadsorption equilibria and selectivities," The Journal of Physical Chemistry B, 1997. 101(24): p. 4798-4802.

[46] LEE, J., et al., "Modeling and simulation of a simulated moving bed for adsorptive para-xylene separation," Korean Journal of Chemical Engineering, 2010. 27(2): p. 609-618.

[47] TOURANI, S., et al., "Equilibrium modeling of xylene adsorption on molecular sieves," Fluid Phase Equilibria, 2010. 298(1): p. 54-59.

[48] MELLOT, C., et al., "Adsorption of Gaseous P- or M-Xylene in Bax Zeolite - Correlation between Thermodynamic and Crystallographic Studies," Langmuir, 1995. 11(5): p. 1726-1730.

[49] PICHON, C., et al. *Location of Water and p-Xylene Molecules Adsorbed on Hydrated Zeolite BaX–A Low-Temperature Neutron Powder Diffraction Study*. in *Materials Science Forum*. 2004. Trans Tech Publ.

[50] LANDA, H. O. R., D. FLOCKERZI, and A. SEIDEL-MORGENSTERN, "A method for efficiently solving the IAST equations with an application to adsorber dynamics," AIChE Journal, 2013. 59(4): p. 1263-1277.

[51] GAMBA, G., et al., "Adsorption Equilibria of Nonideal Multicomponent Systems at Saturation," Aiche Journal, 1990. 36(11): p. 1736-1742.

[52] DO, D. D., *Adsorption Analysis: Equilibria and Kinetics:(With CD Containing Computer Matlab Programs)*. Vol. 2. 1998: World Scientific.

[53] MINCEVA, M. and A. E. RODRIGUES, "Influence of the transfer line dead volume on the performance of an industrial scale simulated moving bed for p-xylene separation," Separation science and technology, 2003. 38(7): p. 1463-1497.

[54] FOURER, R., D. M. GAY, and B. W. KERNIGHAN, *AMPL: A mathematical programming language*. 1987: Citeseer.

[55] WAECHTER, A., et al., "Introduction to IPOPT: A tutorial for downloading, installing, and using IPOPT". 2009, Revision.

[56] TIE, S., et al., "Model-based design and experimental validation of simulated moving bed reactor for production of glycol ether ester," Chemical Engineering Journal, 2016. 301: p. 188-199.

[57] BENTLEY, J. and Y. KAWAJIRI, "Prediction-correction method for optimization of simulated moving bed chromatography," AIChE Journal, 2013. 59(3): p. 736-746.

[58] GEE, J. A., et al., "Computational Identification and Experimental Evaluation of Metal-Organic Frameworks for Xylene Enrichment," The Journal of Physical Chemistry C, 2015.

[59] KOH, D. Y., et al., "Reverse osmosis molecular differentiation of organic liquids using carbon molecular sieve membranes," Science, 2016. 353(6301): p. 804-807.

[60] JIN, W. and P. C. WANKAT, "Hybrid Simulated Moving Bed Processes for the Purification of p-Xylene," Separation Science and Technology, 2007. 42(4): p. 669-700.

[61] HESS, W. T., A. KURTZ, and D. STANTON, "Kirk-Othmer encyclopedia of chemical technology," Kirk-Othmer (Ed.) John Wiley & Sons Ltd., New York, 1995.

[62] LI, P., G. XIU, and A. E. RODRIGUES, "Proteins separation and purification by salt gradient ion-exchange SMB," AIChE journal, 2007. 53(9): p. 2419-2431.

[63] LONG, N. V. D., et al., "Solvent-gradient SMB to separate o-xylene and p-xylene," Korean Journal of Chemical Engineering, 2011. 28(4): p. 1110-1119.

[64] GUO, S., et al., "A concurrent approach for process design and multicomponent adsorption modeling with local isotherms," Chemical Engineering Science, 2017. 171: p. 426-439.

[65] BENTLEY, J., C. SLOAN, and Y. KAWAJIRI, "Simultaneous modeling and optimization of nonlinear simulated moving bed chromatography by the prediction–correction method," Journal of Chromatography A, 2013. 1280: p. 51-63.

[66] KIWALA, D., et al., "Center-cut separation of intermediately adsorbing target component by 8-zone simulated moving bed chromatography with internal recycle," Journal of Chromatography A, 2016. 1453: p. 19-33.